One-loop expressions for $H^{\pm} \to W^{\pm}Z$ and their implications at muon-TeV colliders*

Dzung Tri Tran[1,2] Quang Hoang-Minh Pham[3] Khoa Ngo-Thanh Ho[3] Khiem Hong Phan[1,2†]

[1]Institute of Fundamental and Applied Sciences, Duy Tan University, Ho Chi Minh City 70000, Vietnam
[2]Faculty of Natural Sciences, Duy Tan University, Da Nang City 50000, Vietnam
[3]VNUHCM-University of Science, 227 Nguyen Van Cu, District 5, Ho Chi Minh City 700000, Vietnam

Abstract: One-loop contributions for the decay process $H^{\pm} \to W^{\pm}Z$ within the Two-Higgs-Doublet Model (THDM) are computed in the general $\mathcal{R}_{\xi}$ gauge, and its phenomenological applications at future muon–TeV colliders are investigated. Analytic results are confirmed by several consistency tests, including those of ξ-independence, renormalization-scale stability, and the ultraviolet finiteness of the one-loop amplitude. We first perform an updated parameter scan of the Type-X THDM in phenomenological studies. The production of charged Higgs boson pairs at future muon–TeV colliders is then investigated through two processes: $\mu^+\mu^- \to H^+H^- \to W^{\pm}W^{\mp}Zh$ and $\mu^+\mu^- \to \gamma\gamma \to H^+H^- \to W^{\pm}W^{\mp}Zh$. Both signal events and their significance are evaluated considering the corresponding Standard Model backgrounds. We find that the signal significances can exceed 5σ at several benchmark points in the viable parameter space of the Type-X THDM.

Keywords: one-loop corrections, Higgs phenomenology, physics beyond the Standard Model, physics at present and future colliders

DOI: 10.1088/1674-1137/ae2660 **CSTR:** 32044.14.ChinesePhysicsC.50033108

I. INTRODUCTION

Searches for additional scalar Higgs boson productions in many extensions of the Standard Model (SM) are a key motivation for the construction of future colliders, including the High-Luminosity LHC (HL-LHC) and proposed lepton colliders such as the International Linear Collider (ILC) and muon–TeV colliders. The discovery of the additional scalar Higgs bosons would provide direct evidence for new physics and would also offer enhanced insight into the dynamics of electroweak symmetry breaking (EWSB). In all possible production channels of exotic scalar states, singly charged Higgs boson productions have recently received particular attention at colliders. Experimentally, searches for charged Higgs bosons in the light mass regions produced in top-quark decay have been detected at $\sqrt{s} = 7$ and 8 TeV at the LHC [1−4]. The ATLAS collaboration has pursued additional explorations of charged Higgs bosons following decay channels $H^+ \to \tau\nu$ [5] and $H^+ \to c\bar{s}$ [6]. For heavier charged Higgs states, both ATLAS and CMS have conducted searches through decay channels such as $H^{\pm} \to tb$ [7−9], $H^{\pm} \to W^{\pm}Z$ [10, 11] at $\sqrt{s} = 8$ TeV, and via vector boson fusion production at $\sqrt{s} = 13$ TeV [12]. Furthermore, searches for $H^{\pm} \to cb/cs$ at $\sqrt{s} = 8$ TeV have been reported in Refs. [13, 14], while the $H^{\pm} \to HW^{\pm}$ decay mode has been studied at $\sqrt{s} = 13$ TeV [15, 16]. More recently, both ATLAS and CMS investigated charged Higgs bosons in association with top quarks and in top-quark decay, wherein both production channels were analyzed with the subsequent decay $H^{\pm} \to \tau^{\pm}\nu_{\tau}$ [17−19].

Theoretically, charged Higgs boson production at the LHC has been calculated within many BSM scenarios. In THDM, $pp \to tH^- \to tW^-b\bar{b}$ production has been computed, including top-quark polarization effects as discussed in Ref. [20, 21]. Additionally, the decay $H^+ \to t\bar{b}$ has been systematically examined in the Minimal Supersymmetric SM (MSSM) [22]. The production of charged Higgs boson pairs at the HL-LHC has been investigated in Ref. [23]. Charged Higgs bosons in the light-mass regions decaying into electroweak vector bosons have been analyzed based on Run III data [24]. Investigations of the productions for $pp \to H^{\pm}h/A$ and $pp \to H^+H^-$ with $H^{\pm} \to W^{\pm}h/A$ have been carried out in Ref. [25]. Further

Received 30 September 2025; Accepted 2 December 2025; Accepted manuscript online 3 December 2025

* This research is funded by Vietnam National Foundation for Science and Technology Development (NAFOSTED) (103.01-2023.16)

† E-mail: phanhongkhiem@duytan.edu.vn

studies on charged Higgs bosons at the LHC have been reported in Refs. [26–28], including analyses of production via vectorlike top-quark pairs [29–34] and studies on the $W\gamma$ decay mode [35]. Production of charged Higgs bosons at future lepton colliders has been studied at $\mu^+\mu^-$ and e^+e^- machines [36–39]. Moreover, heavy charged Higgs states at $\gamma\gamma$ colliders have been probed using multivariate analyses including the $H^\pm \to W^\pm H$ decay channel [40, 41]. Ref. [42] has shown that new physics effects from scalar Higgs exchange in the loop can be probed through electroweak corrections to the process $e^-e^+ \to h\nu_e\nu_e$ at e^+e^- machines.

In comparison with hadron colliders, muon–TeV colliders provide a clean leptonic collision environment for high-precision tests, similar to e^-e^+ collisions. Moreover, they also open the door to a high-energy frontier from which to probe physics beyond the SM [43, 44]. Given that the mass of the muon is greater than that of the the electron by a factor of roughly 207, the contributions of neutral-Higgs exchange in the s-channel may be enhanced due to resonance effects. Last but not least, the coupling of charged scalar Higgs bosons to muons is proportional to $\tan\beta$ or $\cot\beta$ depending on the type of THDM. As a result, these effects could provide an opportunity to distinguish among the four types of THDM. Second, loop–induced decay $H^\pm \to W^\pm Z$ is sensitive to BSM effects and provides important information for discriminating among different types of THDM. This decay process was computed in Ref. [45]. Alternative calculations including the CP-violating THDM have been presented in Refs. [46–50]. In this work, one-loop contributions for decay $H^\pm \to W^\pm Z$ in THDM are computed and their implications for future muon–TeV colliders are studied. In contrast to other works, our calculations are performed in the general $\mathcal{R}_\xi$ gauge and the results are verified through several self-consistency checks such as the ξ-independence, renormalization-scale stability, and ultraviolet (UV) finiteness of the amplitude. Many previous studies have shown [51] that charged Higgs masses vary widely from $O(100)$ GeV to approximately1000 GeV in Type-I and Type-X of THDM, whereas they are typically greater than 500 GeV in the other types of THDM. Thus, the Type-I and Type-X models are of particular interest in searching for charged Higgs bosons in the low-mass regions, especially around the $m_W + m_Z$ threshold. We emphasize that the phenomenological results for the Type-I case were presented in our previous work [52]. In this paper, we present a phenomenological analysis of the Type-X THDM based on an updated viable parameter space. Charged Higgs pair production is then studied via $\mu^+\mu^- \to H^+H^- \to W^\pm W^\mp Zh$ and $\mu^+\mu^- \to \gamma\gamma \to H^+H^- \to W^\pm W^\mp Zh$, with signals evaluated with respect to the SM backgrounds.

The remainder of this paper is structured as follows. In Section II, we review the THDM framework, its constraints, and the updated parameter-space scan for the Type-X THDM. In Section III, we present the one-loop calculation of $H^\pm \to W^\pm Z$ along with numerical checks of the computation. We then discuss the phenomenological applications in Section IV. Section V concludes by summarizing our findings. Analytic expressions and checks of ξ-independence are provided in the appendices.

II. THDM AND ITS CONTRAINTS

A detailed review of THDM can be found in Ref. [53]. It is shown that tree-level flavor-changing neutral currents can be prevented by applying a discrete Z_2 symmetry in the Lagrangian, as discussed in Ref. [53]. The different charge quantum numbers of the Z_2 for scalar doublets and fermion fields lead to four distinct Yukawa types (known as Type-I, II, X, Y) (see also Ref. [54] for more detail). The Yukawa Lagrangian can be parameterized as

$$\begin{aligned}\mathcal{L}_{\rm Y} =& -\sum_{f=u,d,\ell}\left(\sum_{\phi_j=h,H} g_{\phi_j ff}\cdot\phi_j\bar{f}f + g_{Aff}\cdot A\bar{f}\gamma_5 f\right)\\ &-\left[\bar{u}_i\left(g^L_{H^+u_id_j}m_{u_i}P_L + g^R_{H^+u_id_j}m_{d_j}P_R\right)d_jH^+\right]\\ &+\cdots \end{aligned} \tag{1}$$

$$\begin{aligned}=& -\sum_{f=u,d,\ell}\left(\sum_{\phi_j=h,H}\frac{m_f}{v}\xi^f_{\phi_j}\phi_j\bar{f}f - {\rm i}\frac{m_f}{v}\xi^f_A\bar{f}\gamma_5 fA\right)\\ &-\frac{\sqrt{2}}{v}\left[\bar{u}_iV_{ij}\left(m_{u_i}\xi^u_AP_L + \xi^d_Am_{d_j}P_R\right)d_jH^+\right]\\ &-\frac{\sqrt{2}}{v}\bar{\nu}_L\xi^\ell_Am_\ell\ell_RH^+ + {\rm H.c.}\end{aligned} \tag{2}$$

In the Lagrangian, the CKM matrix elements are denoted by V_{ij}, $\ell_{L/R}(\nu_{L/R})$ represents the left- and right-handed lepton fields, and $P_{L/R} = (1\mp\gamma_5)/2$ denotes the projection operators. It is easy to check whether the vertices of the charged Higgs with up- and down-type quarks depend linearly on $\cot\beta$ in the Type-X THDM. As a result, fermionic loop contributions are thus diminished in the large-t_β regime.

We now turn to the theoretical and experimental bounds on THDM. Theoretical bounds are obtained by imposing conditions such as perturbative unitarity, perturbativity, and vacuum stability, all of which are taken into account in the models under consideration. In the experimental limits, the measured data of the SM-like Higgs properties, the data of flavor observables, and electroweak precision tests are taken into consideration in the constraints. We refer to our previous work [52] for fur-

ther details about these conditions, wherein the Type-I THDM was studied in greater detail. The parameter space is scanned as follows. We choose parameters for the Type-X THDM within the ranges of $s_{\beta-\alpha} \in [0.97,1]$, $t_\beta \in [0.5,45]$, $m_H \in [130,1000]$ GeV, $m_{A,H^\pm} \in [130,1000]$ GeV, and $m_{12}^2 \in [0,10^6]$ GeV^2, with the SM-like Higgs mass fixed at $m_h = 125.09$ GeV. The sampling points are first tested against theoretical constraints. The allowed points are then checked with the Electroweak Precision Observables (EWPOs). The surviving parameter space is subsequently passed to `HiggsBounds-5.10.1` [55] and `HiggsSignals-2.6.1` [56] to incorporate collider limits and Higgs precision measurement data, respectively. It is important to stress that both `HiggsBounds-5.10.1` and `HiggsSignals-2.6.1` are incorporated into `2HDMC` [57]. Finally, the remaining points are evaluated with `SuperIso v4.1` [58] to include flavor constraints. After all conditions are imposed, the viable parameter space is thoroughly examined as discussed below. In Fig. 1, the left panel shows the scatter plot of the viable parameter space in the $(m_A, m_H, m_{H^\pm})$ plane, whereas the right panel displays the scatter plot in the $(m_{12}^2, m_{H^\pm}, t_\beta)$ plane. The results indicate that the data favor the mass region $m_A > m_{H^\pm} = m_H$ over other mass patterns. Across the full charged Higgs mass range, parameter regions with $t_\beta \leq 10$ and larger m_{12}^2 values are preferred, as shown in the right panel.

III. ONE-LOOP–INDUCED EXPRESSIONS FOR $H^\pm \to W^\pm Z$ IN THE GENERAL R_ξ

In this work, we follow the method developed in Refs. [46, 47] and extend them for calculating the considered processes in the general $\mathcal{R}_\xi$ gauge. Furthermore, we go beyond previous works by presenting the first results verified through several self-consistency checks, such as those of ξ-independence, renormalization-scale stability, and the ultraviolet finiteness of the amplitude. As shown in Refs. [46, 47], all one-loop Feynman diagrams for this decay process in the 't Hooft–Feynman gauge are taken into account in the decay rate, and the effects of renormalization schemes on the obtained results are negligible. Thus, the effects of renormalization schemes are also neglected in this work.

First, all one-loop Feynman diagrams are generated in the general R_ξ gauge and are shown explicitly in Appendix C. The decay amplitude for $H^\pm(p) \to W_\mu^\pm(p_1) Z_\nu(p_2)$ can be expressed via the form factors $\mathcal{T}_i$ $(i = 1,2,3)$ following the corresponding Lorentz structures.

$$\mathcal{M}_{H^\pm \to W^\pm Z} = \left[g^{\mu\nu}\mathcal{T}_1 + p_2^\mu p_1^\nu \mathcal{T}_2 + \mathrm{i}\,\epsilon^{\mu\nu\rho\sigma} p_{1,\rho}\, p_{2,\sigma}\, \mathcal{T}_3 \right] \varepsilon_\mu^*(p_1)\varepsilon_\nu^*(p_2). \tag{3}$$

where $\epsilon^{\mu\nu\rho\sigma}$ is the completely antisymmetric tensor, p (p_1 and p_2) is the ingoing (outgoing) momentum, and ε_μ^* (ε_ν^*) are the polarization vectors for external $W^\pm$ and Z bosons, respectively. In the above formulas, two relations for on-shell vector bosons $p_1^\mu \varepsilon_\mu^*(p_1) = p_2^\nu \varepsilon_\nu^*(p_2) = 0$ have been utilized for our calculations.

The corresponding form factors $\mathcal{T}_i$ are decomposed into one-loop fermionic ($\mathcal{T}_i^F$) and bosonic ($\mathcal{T}_i^B$) contributions. The factors are computed from the respective groups of Feynman diagrams as follows:

$$\mathcal{T}_i^{(F/B)} = \mathcal{T}_{i,\mathrm{Trig}}^{(F/B)} + \mathcal{T}_{i,\mathrm{Self}}^{(F/B)} + \mathcal{T}_{i,\mathrm{Tad}}^{(F/B)}. \tag{4}$$

The index notations F/B indicate the corresponding contributions from fermion and boson loops. The quantities $\mathcal{T}_{i,\mathrm{Trig/Self/Tad}}^{(F/B)}$ are obtained from the triangle, self-energy, and tadpole Feynman diagrams, respectively.

Analytical results for $\mathcal{T}_{i,\mathrm{Trig/Self/Tad}}^{(F/B)}$ in the $\mathcal{R}_\xi$ gauge are presented using scalar Passarino-Veltman functions (PV-functions) [59] in Appendix A, whereas analytical checks of ξ-gauge invariance are provided in Appendix B. In this

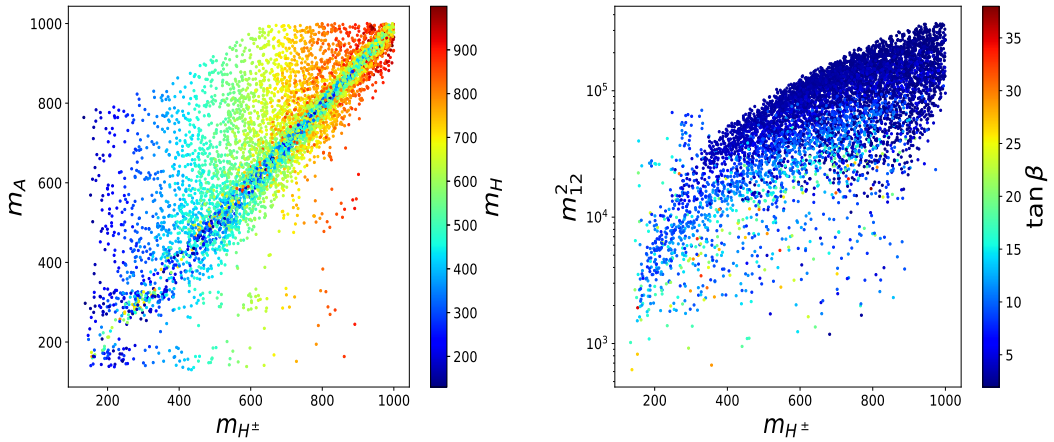

Fig. 1. (color online) Scatter plots showing correlations in the parameter space: $(m_A, m_{H^\pm}, m_H)$ in the left panel and $(m_{12}^2, m_{H^\pm}, t_\beta)$ in the right panel.

section, we describe the numerical checks of the self-consistency of the one-loop form factors, including their ξ-independence, UV finiteness, and stability under variations in the renormalization scale μ^2. Specifically, for ξ-gauge invariance, we examine only the form factors $\mathcal{T}^B_{1,2}$ arising from boson-loop contributions, where ξ_W and ξ_Z are varied in comparison with the case $\xi_{W/Z}=1$ in the 't Hooft–Feynman gauge. For illustration, we adopt representative THDM parameters: $m_{H^\pm}=m_H=800\,\text{GeV}$, $m_A=m_{H^\pm}+m_Z$, $s_{\beta-\alpha}=0.98$ and the scale of the Z_2-symmetry $m^2_{12}=5\cdot10^4\,\text{GeV}^2$. The results of these checks are summarized in Tables 1, 2, where ξ_W and ξ_Z are varied over wide ranges. These results demonstrate good numerical stability.

We then perform numerical checks of the C_{UV}- and μ^2-independence (See Appendix A for the definitions of these parameters.) for the form factors $\mathcal{T}_i=\mathcal{T}^F_i+\mathcal{T}^B_i$ with $i=1,2,3$. We note that the total one-loop form factor should be considered in these tests, with gauge parameters fixed at $\xi_W=\xi_Z=100$ for example. It should also be noted that the fermion-loop contribution $\mathcal{T}^F_1$ is evaluated in the Type-X THDM as an illustrative example. The numerical results for these tests are obtained using the same parameter point as specified above. By varying C_{UV} and μ^2 over wide ranges, the results demonstrate good numerical stability (see Tables 3, 4, 5).

After collecting all the necessary one-loop form factors and performing the self-consistency checks, the decay rates are computed in terms of these form factors.

$$\Gamma_{H^\pm\to W^\pm Z}=\frac{\sqrt{\Lambda(\mu_W,\mu_Z)}}{128\pi\cdot m_{H^\pm}}\left\{4\left|\mathcal{T}_1\right|^2+m^4_{H^\pm}\Lambda(\mu_W,\mu_Z)\left|\mathcal{T}_3\right|^2+\frac{m^4_{H^\pm}}{16m^2_Wm^2_Z}\left|2\left(1-\mu_W-\mu_Z\right)\mathcal{T}_1+m^2_{H^\pm}\Lambda(\mu_W,\mu_Z)\mathcal{T}_2\right|^2\right\}. \tag{5}$$

The relevant kinematical variables are $\mu_V=m^2_V/m^2_{H^\pm}$ for $V=W,Z$, and the kinematical function $\Lambda(x,y)$ is defined as $\Lambda(x,y)=(1-x-y)^2-4xy$.

IV. PRODUCTION OF SINGLY CHARGED HIGGS BOSONS AT MUON–TEV COLLIDERS

Singly charged Higgs boson production at muon–TeV colliders is investigated in this section. For the phenomenological analysis, we use the following benchmark configuration: $s_{\beta-\alpha}=0.98$, $m_A=m_{H^\pm}+m_Z=m_H+m_Z$, and $m^2_{12}=5\times10^4\,\text{GeV}^2$. The charged Higgs mass is scanned over the range $200\,\text{GeV}\le m_{H^\pm}\le1000\,\text{GeV}$, whereas while the mixing parameter is set as $2\le t_\beta\le12$. All other SM parameters are taken from the Particle Data Group [60].

A. Branching fractions

We first evaluate the branching fractions of the charged Higgs boson in the Type-X THDM. The one-loop–induced process $H^\pm\to W^\pm\gamma$ has already been reported in our previous work [52], whereas decay mode $H^\pm\to W^\pm Z$ is considered in this work. The remaining decay channels are taken from Ref. [48]. In Fig. 2, the branching fractions of the charged Higgs boson are shown for all considered decay modes within the interval $200\,\text{GeV}\le m_{H^\pm}\le1000\,\text{GeV}$. At $t_\beta=2$, the tb and Wh channels are the leading contributions, whereas the branching ratio of $H^\pm\to W^\pm Z$ remains of the order 10^{-4} across the entire mass range. For $t_\beta=4$, the tb and Wh channels continue to dominate; however, the $H^\pm\to W^\pm Z$ mode remains around $\sim10^{-4}$. Next, we consider the branching fractions at $t_\beta=8$. We find that the branching ratio of $H^\pm\to W^\pm Z$ increases to the order of 10^{-2} in the low-mass region but decreases to about 10^{-3} at higher

Table 1. Numerical checks of R_ξ gauge invariance for the form factor $\mathcal{T}^B_1$ in boson-loop contributions are performed by varying the ξ_W and ξ_Z values and by comparing them with the case $\xi_{W/Z}=1$ in the 't Hooft–Feynman gauge. We take the THDM parameters as follows: the Higgs masses $m_{H^\pm}=m_H=800$ GeV, $m_A=m_{H^\pm}+m_Z$, $s_{\beta-\alpha}=0.98$, $t_\beta=10$, and the scale of the Z_2-symmetry $m^2_{12}=5\cdot10^4$ GeV^2.

(ξ_W,ξ_Z)	$(1,1)$	$(10,10^2)$	$(10^3,10^4)$
$\sum_\phi\mathcal{T}^{B,\phi-A}_{1,\text{Trig}}$	$-50.72721116+0\text{i}$	$-50.79862234+0\text{i}$	$-51.65760847+0\text{i}$
$\sum_\phi\mathcal{T}^{B,\phi-H^\pm}_{1,\text{Trig}}$	$50.66247519+0\text{i}$	$50.66247519+0\text{i}$	$50.66247519+0\text{i}$
$\sum_\phi\mathcal{T}^{B,\phi-W^\pm}_{1,\text{Trig}}$	$4.197968064-1.192202277\text{i}$	$3.885889625-0.7864121884\text{i}$	$9.769973063+2.88619913\text{i}$
$\sum_\phi\mathcal{T}^{B,\phi-Z}_{1,\text{Trig}}$	$0.0173173496+0\text{i}$	$0.3215636277+0\text{i}$	$1.42510883+0\text{i}$
$\sum_\phi\mathcal{T}^{B,\phi-W^\pm Z}_{1,\text{Trig}}$	$-4.072882533+1.271771141\text{i}$	$-3.945505715+0.815048537\text{i}$	$-10.70487047-3.318528531\text{i}$
$\mathcal{T}^B_{1,\text{Self}}$	$69.46890566-0.023317639\text{i}$	$78.17143601+0.027614876\text{i}$	$-30.76307909+0.4885806253\text{i}$
$\mathcal{T}^B_{1,\text{Tad}}$	$-69.69069235+0\text{i}$	$-78.44135618+0\text{i}$	$31.12388118+0\text{i}$
$\mathcal{T}^B_1$ in Eq. (28)	$-0.1441197805+0.0562512244\text{i}$	$-0.1441197805+0.0562512244\text{i}$	$-0.1441197808+0.0562512244\text{i}$

Table 2. Numerical checks of R_ξ gauge invariance for the form factor $\mathcal{T}_2^B$ in boson-loop contributions are performed by varying the gauge parameters ξ_W and ξ_Z. We take the THDM parameters as follows: the Higgs masses $m_{H^\pm} = m_H = 800$ GeV, $m_A = m_{H^\pm} + m_Z$, $s_{\beta-\alpha} = 0.98$, $t_\beta = 10$, and the scale of the Z_2-symmetry $m_{12}^2 = 5\times10^4$ GeV^2.

(ξ_W, ξ_Z)	$(1,1)$	$(10, 10^2)$	$(10^3, 10^4)$
$\sum_\phi \mathcal{T}^{B,\phi-A}_{2,\text{Trig}}$	$8.875933961\cdot10^{-7}+0\text{i}$	$8.875933961\cdot10^{-7}+0\text{i}$	$8.875933958\cdot10^{-7}+0\text{i}$
$\sum_\phi \mathcal{T}^{B,\phi-H^\pm}_{2,\text{Trig}}$	$-4.259326679\cdot10^{-7}+0\text{i}$	$-4.259326679\cdot10^{-7}+0\text{i}$	$-4.259326683\cdot10^{-7}+0\text{i}$
$\sum_\phi \mathcal{T}^{B,\phi-W^\pm}_{2,\text{Trig}}$	$3.525339605\cdot10^{-7}+5.18767908\cdot10^{-7}\text{i}$	$3.525339607\cdot10^{-7}+5.18767908\cdot10^{-7}\text{i}$	$3.52533961\cdot10^{-7}+5.1876791\cdot10^{-7}\text{i}$
$\sum_\phi \mathcal{T}^{B,\phi-Z}_{2,\text{Trig}}$	$-7.0029171\cdot10^{-8}+0\text{i}$	$-7.0029171\cdot10^{-7}+0\text{i}$	$-7.0029174\cdot10^{-7}+0\text{i}$
$\sum_\phi \mathcal{T}^{B,\phi-W^\pm Z}_{2,\text{Trig}}$	$-8.244771\cdot10^{-7}-4.926311\cdot10^{-7}\text{i}$	$-8.244771\cdot10^{-7}-4.926311\cdot10^{-7}\text{i}$	$-8.244773\cdot10^{-7}-4.926313\cdot10^{-7}\text{i}$
$\mathcal{T}^B_{2,\text{Self}}$	0	0	0
$\mathcal{T}^B_{2,\text{Tad}}$	0	0	0
$\mathcal{T}_2^B$ in Eq. (28)	$-8.031155\cdot10^{-8}+2.6136808\cdot10^{-8}\text{i}$	$-8.031155\cdot10^{-8}+2.6136809\cdot10^{-8}\text{i}$	$-8.031154\cdot10^{-8}+2.613682\cdot10^{-8}\text{i}$

Table 3. Numerical checks of C_{UV} and the renormalization scale μ^2 are performed for the form factors $\mathcal{T}_1 = \mathcal{T}_1^F + \mathcal{T}_1^B$. The bosonic contribution $\mathcal{T}_1^B$ is evaluated at $\xi_W = \xi_Z = 100$, while the fermionic contribution $\mathcal{T}_1^F$ is calculated in the Type-X THDM. For this analysis, we adopt the following set of THDM parameters: $m_{H^\pm} = m_H = 500$ GeV, $m_A = m_{H^\pm} + m_Z$, $s_{\beta-\alpha} = 0.98$, $t_\beta = 5$, $m_{12}^2 = 5\times10^4$ GeV^2.

(C_{UV}, μ^2)	$(0,1)$	$(10^4, 10^6)$	$(10^6, 10^8)$
$\mathcal{T}^B_{1,\text{Trig}}$	$0.0409007639-0.12057752761\text{i}$	$0.0409007639-0.12057752761\text{i}$	$0.04090076301-0.12057752761\text{i}$
$\mathcal{T}^B_{1,\text{Self}}$	$-0.9723666455+0.1590201866\text{i}$	$799.5362885+0.1590201866\text{i}$	$79940.92392+0.1590201866\text{i}$
$\mathcal{T}^B_{1,\text{Tad}}$	$1.0786977518+0\text{i}$	$-799.4299574+0\text{i}$	$-79940.81759+0\text{i}$
$\mathcal{T}^B_1$	$0.1472318702+0.03844265898\text{i}$	$0.1472318702+0.03844265898\text{i}$	$0.1472318695+0.03844265898\text{i}$
$\mathcal{T}^F_{1,\text{Trig}}$	$0.4996708114-0.19005144066\text{i}$	$-497.4139502-0.19005144066\text{i}$	$-49723.08395-0.19005144066\text{i}$
$\mathcal{T}^F_{1,\text{Self}}$	$-0.3824890675+0.12113853706\text{i}$	$375.5060921+0.12113853706\text{i}$	$37537.3078+0.12113853706\text{i}$
$\mathcal{T}^F_{1,\text{Tad}}$	$-0.1133787187+0\text{i}$	$121.9116612+0\text{i}$	$12185.77995+0\text{i}$
$\mathcal{T}^F_1$	$0.00380302517-0.06891290359\text{i}$	$0.00380302517-0.06891290359\text{i}$	$0.00380302519-0.06891290359\text{i}$
$\mathcal{T}_1 = \mathcal{T}_1^F + \mathcal{T}_1^B$	$0.1510348954-0.03047024446\text{i}$	$0.1510348954-0.03047024446\text{i}$	$0.1510348947-0.03047024446\text{i}$

masses. Finally, we examine the case of $t_\beta = 12$. The results show that the $H^\pm \to W^\pm Z$ branching ratio can reach the order of 10^{-1} in the low-mass region, whereas it remains at the level of 10^{-4} for larger charged Higgs masses. As indicated in the previous section, the fermionic-loop contributions are suppressed in the high-t_β regime. The interference between the fermionic- and bosonic-loop contributions is small and has the opposite sign compared with the squared bosonic contributions. As a result, the decay rates of the $H^\pm \to W^\pm Z$ mode are enhanced in the high-t_β region compared with the small-t_β regime.

B. Processes $\mu^+\mu^- \to H^+H^- \to W^\pm W^\mp Zh$

We investigate the potential to probe charged Higgs pair production by analyzing the process $\mu^+\mu^- \to H^+H^- \to W^\pm W^\mp Zh$ at muon–TeV colliders. It is well known that initial-state radiation (ISR) effects play a crucial role at future lepton colliders. These effects must be taken into account to simulate the signals of the charged Higgs as well to evaluate the corresponding SM backgrounds. By applying the factorization theorems for soft and collinear singularities, the ISR contributions to charged Higgs pair production can be calculated using the master formula

$$\mathrm{d}\sigma(s) = \int \mathrm{d}x_1\mathrm{d}x_2 D(x_1,s)D(x_2,s)\mathrm{d}\sigma_0(x_1x_2s)\Theta(\text{cuts}). \quad (6)$$

In Eq. (6), $\mathrm{d}\sigma_0$ denotes tree-level differential cross sections for both signals $\mu^-\mu^+ \to H^\pm H^\mp \to W^\pm W^\mp Zh$ and the SM background process $\mu^-\mu^+ \to W^\pm W^\mp Zh$. All tree-level Feynman diagrams for the process $\mu^-\mu^+ \to H^\pm H^\mp$ within THDM are shown in Fig. D1. The partonic cross sections are computed by using `FeynArts/FormCalc` [61]. Θ(cuts) represents the appropriate cuts applied in the simulation, as described explicitly in the following paragraphs. $D(x_2, s)$ is the structure function (SF). Of note, we

Table 4. Numerical checks of C_{UV} and the renormalization scale μ^2 are performed for the form factors $\mathcal{T}_2 = \mathcal{T}_2^F + \mathcal{T}_2^B$. The bosonic contribution $\mathcal{T}_2^B$ is evaluated at $\xi_W = \xi_Z = 100$, while the fermionic contribution $\mathcal{T}_2^F$ is calculated in the Type-X THDM. For this analysis, we adopt the following THDM parameters: $m_{H^\pm} = m_H = 500$ GeV, $m_A = m_{H^\pm} + m_Z$, $s_{\beta-\alpha} = 0.98$, $t_\beta = 5$, and $m_{12}^2 = 5\times10^4$ GeV^2.

(C_{UV},μ^2)	$(0,1)$	$(10^4,10^6)$	$(10^6,10^8)$
$\mathcal{T}_{2,\text{Self}}^B$	0	0	0
$\mathcal{T}_{2,\text{Tad}}^B$	0	0	0
$\mathcal{T}_2^B \equiv \mathcal{T}_{2,\text{Trig}}^B$	$-4.46523589\cdot10^{-7} + 8.283757782\cdot10^{-8}\,\text{i}$	$-4.46523589\cdot10^{-7} + 8.283757782\cdot10^{-8}\,\text{i}$	$-4.465235912\cdot10^{-7} + 8.283757782\cdot10^{-8}\,\text{i}$
$\mathcal{T}_{2,\text{Self}}^F$	0	0	0
$\mathcal{T}_{2,\text{Tad}}^F$	0	0	0
$\mathcal{T}_2^F$	$1.039941873\cdot10^{-7} + 1.445658912\cdot10^{-6}\,\text{i}$	$1.039941873\cdot10^{-7} + 1.445658912\cdot10^{-6}\,\text{i}$	$1.039941873\cdot10^{-7} + 1.445658912\cdot10^{-6}\,\text{i}$
$\mathcal{T}_2 = \mathcal{T}_2^F + \mathcal{T}_2^B$	$-3.425294017\cdot10^{-7} + 1.52849649\cdot10^{-6}\,\text{i}$	$-3.425294017\cdot10^{-7} + 1.52849649\cdot10^{-6}\,\text{i}$	$-3.425294039\cdot10^{-7} + 1.52849649\cdot10^{-6}\,\text{i}$

Table 5. Numerical checks of C_{UV} and the renormalization scale μ^2 are performed for the form factors $\mathcal{T}_3 = \mathcal{T}_3^F + \mathcal{T}_3^B$. The bosonic contribution $\mathcal{T}_3^B$ is evaluated at $\xi_W = \xi_Z = 100$, while the fermionic contribution $\mathcal{T}_3^F$ is calculated in the Type-X THDM as an illustrative example of fermion couplings. For this analysis, we adopt the following THDM parameters: $m_{H^\pm} = m_H = 500$ GeV, $m_A = m_{H^\pm} + m_Z$, $s_{\beta-\alpha} = 0.98$, $t_\beta = 5$, and $m_{12}^2 = 5\times10^4$ GeV^2.

(C_{UV},μ^2)	$(0,1)$	$(10^4,10^6)$	$(10^6,10^8)$
$\mathcal{T}_3^B$	0	0	0
$\mathcal{T}_{3,\text{Self}}^F$	0	0	0
$\mathcal{T}_{3,\text{Tad}}^F$	0	0	0
$\mathcal{T}_3^F$	$3.220832776\cdot10^{-7} - 1.274849257\cdot10^{-6}\,\text{i}$	$3.220832776\cdot10^{-7} - 1.274849257\cdot10^{-6}\,\text{i}$	$3.220832777\cdot10^{-7} - 1.274849257\cdot10^{-6}\,\text{i}$
$\mathcal{T}_3 = \mathcal{T}_3^F + \mathcal{T}_3^B$	$3.220832776\cdot10^{-7} - 1.274849257\cdot10^{-6}\,\text{i}$	$3.220832776\cdot10^{-7} - 1.274849257\cdot10^{-6}\,\text{i}$	$3.220832777\cdot10^{-7} - 1.274849257\cdot10^{-6}\,\text{i}$

use the SF functions from Ref. [62], which were originally applied for electron beams. However, at high-energy regions operating at muon–TeV colliders, these SF functions could also be applied to muon beams. For this reason, we apply the SF functions from Ref. [62] with $m_\ell = m_\mu$ appropriately. The expressions for the SF functions are presented in the following paragraphs. The all-order SF functions, which are valid in the soft-photon limit, are given by

$$D_{GL}(x,s) = \frac{\exp\left[\frac{1}{2}\beta\left(\frac{3}{4}-\gamma_E\right)\right]}{\Gamma\left(1+\frac{1}{2}\beta\right)}\frac{1}{2}\beta(1-x)^{\frac{1}{2}\beta-1}, \tag{7}$$

where

$$\beta = \frac{2\alpha}{\pi}(L-1), \quad L = \ln(s/m_\ell^2). \tag{8}$$

Here, α is the fine-structure constant, and m_ℓ denotes the lepton mass. The symbol Γ represents the Gamma function, and γ_E is the Euler–Mascheroni constant. Photon radiation can be considered in the collinear approximation and through collinear logarithmic enhancements, which are included in the large-β factor. According to Eq. (7), the additive SF function up to third-order expansion terms is expressed as follows [62].

$$\begin{aligned} D_A(x,s) = {} & D_{GL}(x,s) - \frac{1}{4}\beta(1+x) + \frac{1}{32}\beta^2\left[(1+x)(-4\ln(1-x)+3\ln(x)) - 4\frac{\ln x}{1-x} - 5 - x\right] \\ & + \frac{1}{384}\beta^3\left\{(1+x)\left[18\zeta(2) - 6\text{Li}_2(x) - 12\ln^2(1-x)\right] + \frac{1}{1-x}\left[-\frac{3}{2}(1+8x+3x^2)\ln x - 6(x+5)(1-x)\ln(1-x)\right.\right. \\ & \left.\left. - 12(1+x^2)\ln x\ln(1-x) + \frac{1}{2}(1+7x^2)\ln^2 x - \frac{1}{4}(39-24x-15x^2)\right]\right\}. \end{aligned} \tag{9}$$

In this structure function, the Riemann ζ function is taken into account and Li_2 is the dilogarithm functions. Furthermore, the factorized SF function up to third order expansion terms can be obtained as [63, 64]

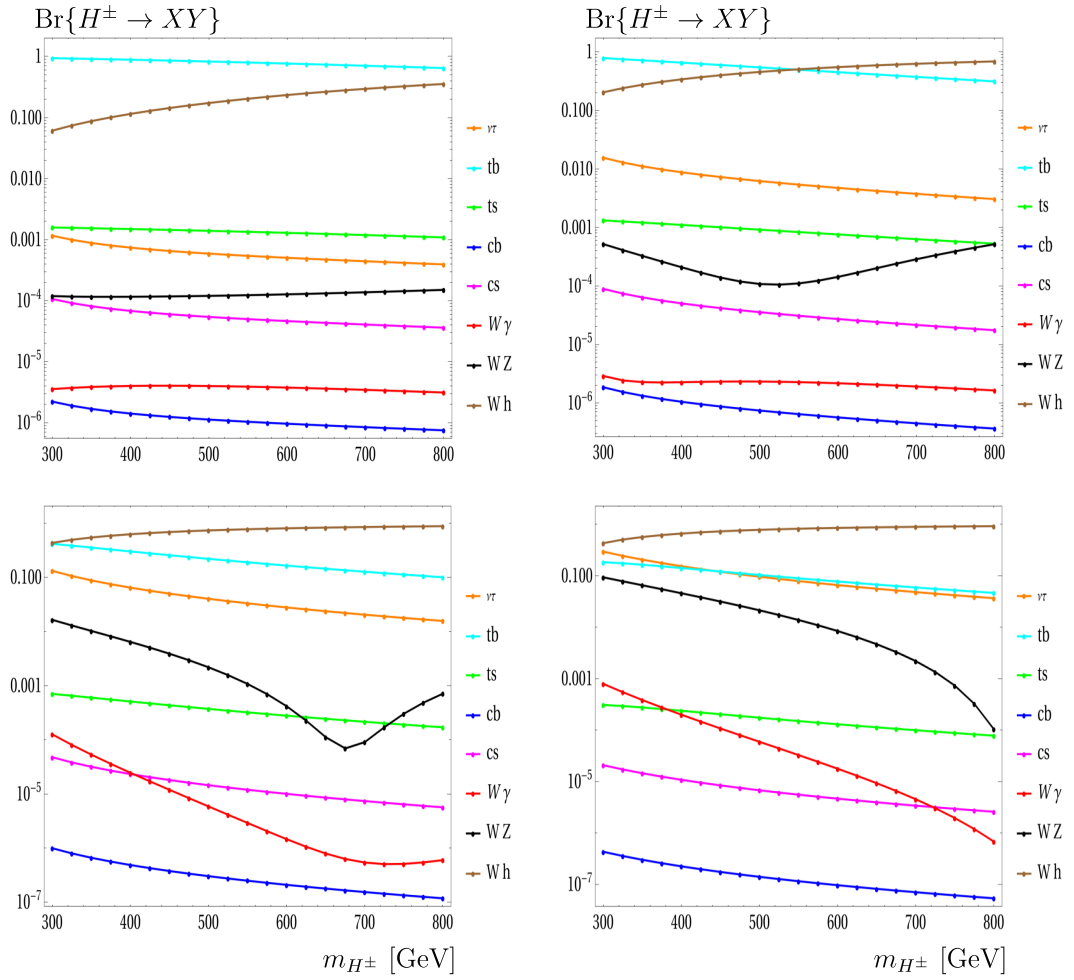

Fig. 2. (color online) Charged Higgs decay branching ratios in the Type-X THDM are shown for the benchmark scenario described above. Each plot is shown for $t_\beta = 2$ (top left), $t_\beta = 4$ (top right), $t_\beta = 8$ (bottom left), and $t_\beta = 12$ (bottom right).

$$
\begin{aligned}
D_F(x,s) &= D_{GL}(x,s) \\
&\times \left\{ \frac{1}{2}(1+x^2) - \frac{\beta}{16}\left[(1+3x^2)\ln x + 2(1-x)^2\right] \right. \\
&+ \frac{\beta^2}{32}\left[(1-x)^2 + \frac{1}{2}(3x^2-4x+1)\ln x \right. \\
&\left. \left. + \frac{1}{12}(1+7x^2)\ln^2 x + (1-x^2)\mathrm{Li}_2(1-x)\right]\right\}.
\end{aligned} \tag{10}
$$

In this work, we consider the ISR effects for both the signal and the SM background processes. The effects of ISR on the scattering process $\mu^+\mu^- \to H^+H^- \to W^{\pm}W^{\mp}Zh$ are examined as functions of the center-of-mass energy (left panel) and of the charged Higgs mass at $\sqrt{s} = 3$ TeV (right panel). In the left plot, we vary the center-of-mass energy from 1000 GeV to 5000 GeV and fix $m_{H^{\pm}} = 300$ GeV with $t_\beta = 8$. We find that the ISR corrections change from approximately -40% to -20%. For the plot shown in the panel at right, we examine the ISR corrections at $\sqrt{s} = 3000$ GeV while varying the charged Higgs mass and fixing $t_\beta = 8$. The results indicate that the corrections range from -20% to -30% for charged Higgs masses in the interval $[300, 600]$ GeV. In Fig. 3, $\sigma_{\rm ISR1}$ ($\sigma_{\rm ISR2}$) denotes the cross-section calculated using the structure functions from Eqs. (9) and (10).

Using the cross section with ISR corrections, we evaluate the signal events for $\mu^+\mu^- \to H^+H^- \to W^{\pm}W^{\mp}Zh$ at $\sqrt{s} = 3$ TeV and the integrated luminosity of 3000 fb^{-1}. The events are generated in the parameter space of $m_{H^{\pm}}$ and the mixing angle t_β as shown in Fig. 4. In this study, we vary $300\,\text{GeV} \le m_{H^{\pm}} \le 600\,\text{GeV}$ and $2 \le t_\beta \le 12$. The results indicate that the signal events are significant in regions of low charged Higgs masses and large t_β values, while in other regions the events become negligible. In the right-panel plot of Fig. 4, the significance of the signals relative to the SM backgrounds is presented at $\mathcal{L} = 500$ fb^{-1}. While the corresponding signal significances are presented at $\mathcal{L} = 1000$ fb^{-1} in the left and at $\mathcal{L} = 3000$ fb^{-1} in the right panel of Fig. 5. The SM background is calculated using the GRACE program [65]. It is emphasized that the SM background also includes the

ISR corrections in the evaluation of the significance. To reduce the SM background, we apply cuts on the invariant masses of the final-state particles: $|m_{Wh} - m_{H^\pm}| < 10$ GeV and $|m_{WZ} - m_{H^\pm}| < 10$ GeV. The significances are shown for $t_\beta = 2$ (green points), $t_\beta = 4$ (yellow points), $t_\beta = 8$ (blue points), and $t_\beta = 12$ (black points). Our results indicate that in the low-mass regions of the charged Higgs, and for $t_\beta = 8$ and 10, the significances can exceed 5σ, while in other regions they become negligible.

Serveral useful points on the systematic uncertainties that might affect the significance are discussed in the following paragraphs. It is well known that the one-loop electroweak radiative corrections to the processes $\mu^+\mu^- \to H^+H^- \to W^\pm W^\mp Zh$ and $\mu^+\mu^- \to W^\pm W^\mp Zh$ can be estimated from the enhancement contributions of the single Sudakov logarithm [66].

$$\delta_W \sim -\frac{\alpha(M_Z^2)}{\pi \sin^2\theta_W} \log\left(\frac{s}{M_Z^2}\right) \sim O(-10\%) \quad \text{at } \sqrt{s} = 3 \text{ TeV}. \tag{11}$$

If weak and ISR corrections are included in the significance calculation, the total electroweak correction can reach approximately $O(-35\%)$. All theoretical uncertainties and detector effects can be incorporated into the systematic uncertainty fraction of the background yield, denoted by ε_B. Consequently, the significance is modified as

$$\mathcal{S} = \frac{N_S}{\sqrt{N_S + \varepsilon_B N_B}}. \tag{12}$$

For example, by taking $\varepsilon_B = 1.3$ and $\varepsilon_B = 1.5$, we verfy wherher the significances vary only slightly due to the small SM background after applying the effective cuts described above. Finally, if we consider the decays $W \to \ell\nu_\ell$ for $\ell = e, \mu, \tau$ with branching fractions of 0.3272, $Z \to b\bar{b}$ with a branching fraction of 0.1512, and $h \to b\bar{b}$ with a branching fraction of 0.53 from the Particle Data Group [60], the significances are subsequently scaled down by a factor of 0.161927, which reduces them to around 5σ at an integrated luminosity of $\mathcal{L} = 3000$ fb^{-1} for the low-mass regions. Details of detector simulations, b-tagging, etc. will be addressed in our future work.

C. Processes $\mu^+\mu^- \to \gamma\gamma \to H^+H^- \to W^\pm W^\mp Zh$

We now turn our attention to another process, $\mu^+\mu^- \to \gamma\gamma \to H^+H^- \to W^\pm W^\mp Zh$. The total cross section is calculated by convoluting the partonic process $\gamma\gamma \to H^+H^- \to W^\pm W^\mp Zh$ with the photon structure function as follows:

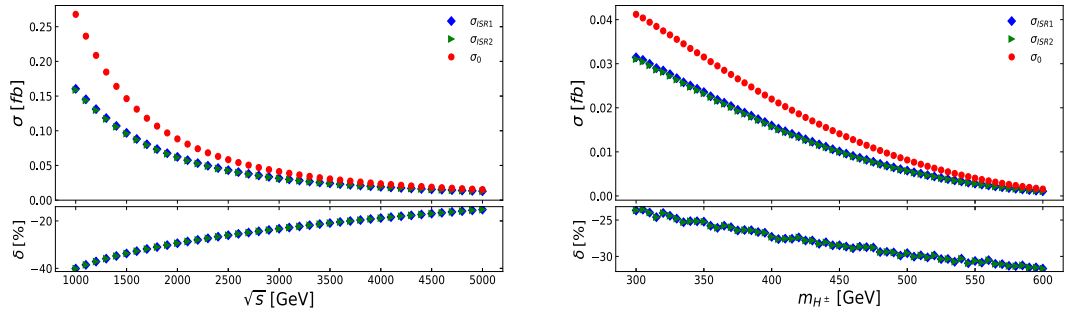

Fig. 3. (color online) Effects of ISR on the scattering process $\mu^+\mu^- \to H^+H^- \to W^\pm W^\mp Zh$ are examined as functions of the center-of-mass energy (left panel) and of the charged Higgs mass at $\sqrt{s} = 3$ TeV (right panel).

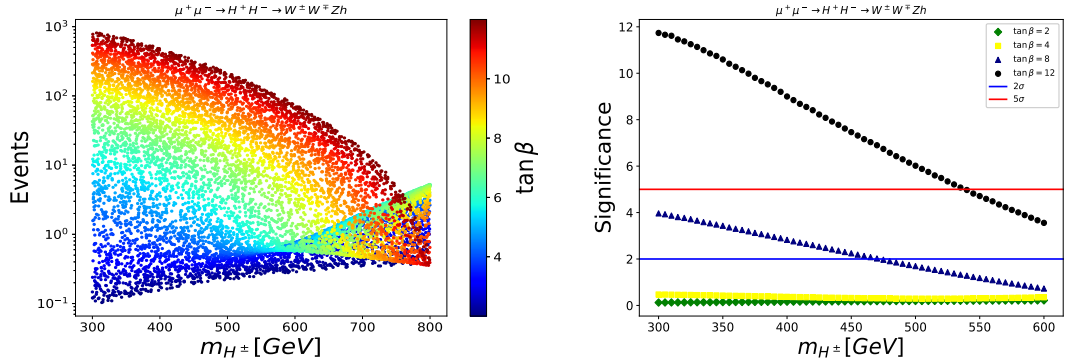

Fig. 4. (color online) Event distributions of the process $\mu^+\mu^- \to H^+H^- \to W^\pm W^\mp Zh$ at an integrated luminosity of $\mathcal{L} = 3000$ fb^{-1} including ISR corrections are shown in the left panel. The corresponding signal significance taking into account the Standard Model backgrounds is presented at $\mathcal{L} = 500$ fb^{-1} in the right panel.

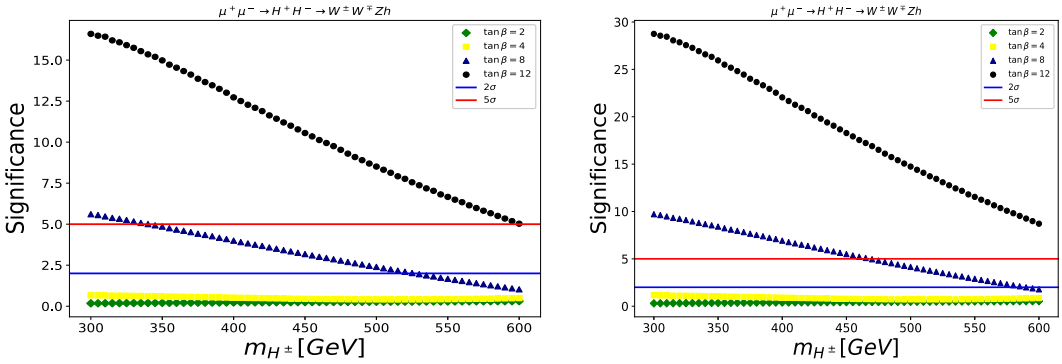

Fig. 5. (color online) The corresponding signal significance taking into account the Standard Model backgrounds, is presented at $\mathcal{L} = 1000$ fb^{-1} in the left and at $\mathcal{L} = 3000$ fb^{-1} in the right panel.

$$\sigma(s) = \int_{\frac{2m_{H^\pm}}{\sqrt{s}}}^{x_{\max}} \mathrm{d}z \left(2z \int_{z^2/x_{\max}}^{x_{\max}} \frac{\mathrm{d}x}{x} f_{\gamma/\mu}(x) f_{\gamma/\mu}\left(z^2/x\right) \right) \hat{\sigma}(\hat{s} = z^2 s). \tag{13}$$

Here, the photon structure function $f_{\gamma/\mu}(x)$ is used, with x denoting the energy fraction of the photon emitted by the incoming lepton. The explicit formulas for $f_{\gamma/\mu}(x)$ are given in [67] with the appropriate of $m_\ell = m_\mu$ as in [68] for example. In the master formulas, we adopt $x_{\max} = 0.83$ as in [69]. All tree-level Feynman diagrams for the process $\gamma\gamma \to H^\pm H^\mp$ within the THDM are shown in Fig. D2. The partonic process $\gamma\gamma \to H^+H^-$ are generated by FeynArts/FormCalc [61]. The SM background which is the process $\gamma\gamma \to W^\pm W^\mp Zh$, is calculated using the the GRACE program [65]. To reduce the SM background, we apply cuts on the invariant masses of the final-state particles: $|m_{Wh} - m_{H^\pm}| < 10$ GeV and and $|m_{WZ} - m_{H^\pm}| < 10$ GeV. In Fig. 6, the numbers of events of the process $\mu^+\mu^- \to \gamma\gamma \to H^+H^- \to W^\pm W^\mp Zh$ at an integrated luminosity of $\mathcal{L} = 3000$ fb^{-1} are shown in the left panel of Fig. 6. The signal significances considering the Standard Model backgrounds are presented at $\mathcal{L} = 500$ fb^{-1} in the right panel of Fig. 6, while the significances are presented at $\mathcal{L} = 1000$ fb^{-1} on the left panel and at $\mathcal{L} = 5000$ fb^{-1} on the right panel of Fig. 7. We observe that the events become significant when the charged Higgs masses are in the low-mass region and $t_\beta = 8, 12$, whereas they are small and can be ignored in other regions. For charged Higgs masses in the low-mass region and $t_\beta = 12$, the significance can exceed 5σ. In other cases, the significances are negligible.

V. CONCLUSIONS

In this article, we have calculated one-loop contributions for the decay process $H^\pm \to W^\pm Z$ in the Two-Higgs-Doublet Model and examined the posibility searches for charged Higgs pair production at future muon–TeV colliders. The computations have been performed in the $\mathcal{R}_\xi$ gauge, and the analytical results were verified through self-consistency tests such as ξ-independence, ultraviolet finiteness, and renormalization-scale stability of the process amplitude. The numerical results demonstrate good stability. We have revisited the parameter scan for the Type-X THDM in the phenomenological results. Based on the updated viable parameter space, we have analyzed charged Higgs pair production at future muon–TeV colliders by considering the processes $\mu^+\mu^- \to H^+H^- \to W^\pm W^\mp Zh$ and $\mu^+\mu^- \to \gamma\gamma \to H^+H^- \to W^\pm W^\mp Zh$. The corresponding signal events and statistical significances were simulated with respect to the relevant SM backgrounds. Our findings show that the signal significance can exceed 5σ at several benchmark points within the viable parameter space of the Type-X THDM.

APPENDIX A: ONE-LOOP FORM FACTORS IN THE GENERAL $\mathcal{R}_\xi$-GAUGE

The conventions for one-loop one-, two-, and three-point tensor integrals with rank P, following Refs. [70, 59, 71], are given by

$$\{A; B; C\}^{\mu_1\mu_2\cdots\mu_P} = (\mu^2)^{2-d/2} \int \frac{\mathrm{d}^d k}{(2\pi)^d} \frac{k^{\mu_1} k^{\mu_2} \cdots k^{\mu_P}}{\{D_1; D_1D_2; D_1D_2D_3\}}. \tag{A1}$$

Here, D_j^{-1} $(j = 1, \cdots, 3)$ are the Feynman propagators defined as

$$D_j = (k + q_j)^2 - m_j^2 + \mathrm{i}\rho, \tag{A2}$$

where $q_j = \sum_{i=1}^{j} p_i$, p_i are the external momenta, and m_j are the internal masses in the loops. Dimensional regularization for one-loop integrals is performed in a space–time dimension $d = 4 - 2\varepsilon$ (the UV-divergent part is isolated as $C_{UV} = 1/\varepsilon + \log(4\pi) - \Gamma_E$, Γ_E is the Euler–Mascheroni constant). In the above expressions, the parameter μ^2 serves as the renormalization scale. Explicit reduction

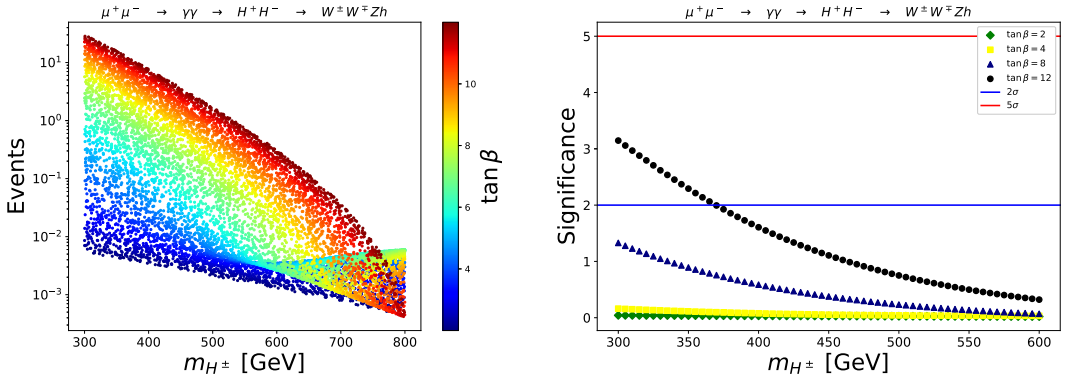

Fig. 6. (color online) The signal events of the process $\mu^+\mu^- \to \gamma\gamma \to H^+H^- \to W^\pm W^\mp Zh$ at an integrated luminosity of $\mathcal{L} = 3000$ fb^{-1} are shown in the left panel. The corresponding signal significance taking into account the SM backgrounds is presented at $\mathcal{L} = 500$ fb^{-1} in the right panel.

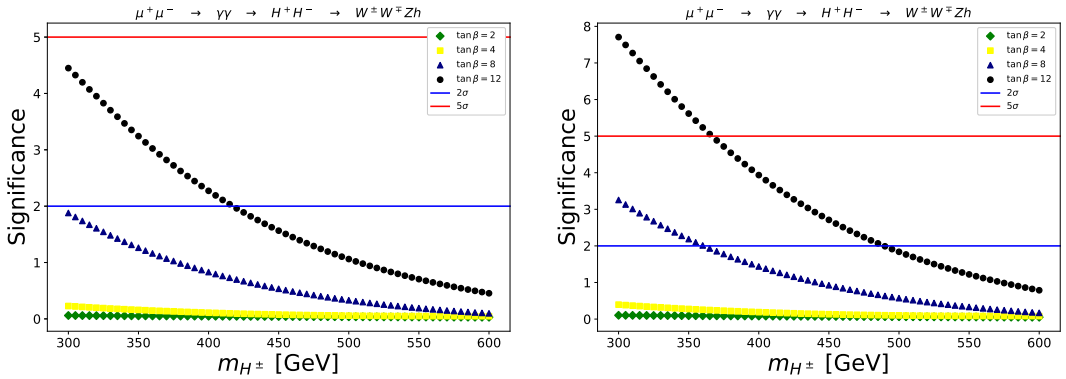

Fig. 7. (color online) The corresponding signal significances taking into account the SM backgrounds are presented at $\mathcal{L} = 1000$ fb^{-1} in the left panel and at $\mathcal{L} = 3000$ fb^{-1} in the right panel.

formulas for one-, two-, and three-point tensor integrals up to rank $P = 3$ are given in Ref. [70].

$$A^\mu = 0, \tag{A3}$$

$$A^{\mu\nu} = g^{\mu\nu}A_{00}, \tag{A4}$$

$$A^{\mu\nu\rho} = 0, \tag{A5}$$

$$B^\mu = q^\mu B_1, \tag{A6}$$

$$B^{\mu\nu} = g^{\mu\nu}B_{00} + q^\mu q^\nu B_{11}, \tag{A7}$$

$$B^{\mu\nu\rho} = \{g,q\}^{\mu\nu\rho}B_{001} + q^\mu q^\nu q^\rho B_{111}, \tag{A8}$$

$$C^\mu = q_1^\mu C_1 + q_2^\mu C_2 = \sum_{i=1}^{2} q_i^\mu C_i, \tag{A9}$$

$$C^{\mu\nu} = g^{\mu\nu}C_{00} + \sum_{i,j=1}^{2} q_i^\mu q_j^\nu C_{ij}, \tag{A10}$$

$$C^{\mu\nu\rho} = \sum_{i=1}^{2}\{g,q_i\}^{\mu\nu\rho}C_{00i} + \sum_{i,j,k=1}^{2} q_i^\mu q_j^\nu q_k^\rho C_{ijk}. \tag{A11}$$

The detailed expressions for these form factors in the general R_ξ gauge are given in the following paragraphs. In the analytical expressions below, we have used the notations given as follows.

$$A_{ij\ldots}(P) = A_{ij\ldots}(M_P^2), \tag{A12}$$

$$B_{ij\ldots}(p^2;P_1,P_2) = B_{ij\ldots}(p^2;M_{P_1}^2,M_{P_2}^2), \tag{A13}$$

$$C_{ij\ldots}(p_1^2,p_2^2,p_3^2;P_1,P_2,P_3) = C_{ij\ldots}(p_1^2,p_2^2,p_3^2;M_{P_1}^2,M_{P_2}^2,M_{P_3}^2). \tag{A14}$$

The analytic formulas for all form factors are ex-

pressed in terms of PV-functions using the adopted shorthand notations as presented below in the following paragraphs.

Form factors $\mathcal{T}^B_{i,\mathrm{Trig}}$*:*

The form factor $\mathcal{T}^B_{i,\mathrm{Trig}}$ $(i=1,2,3)$ is expressed in terms of the main contributions involving scalar Higgs bosons $\phi \equiv h,H$, together with charged particles such as $H^\pm, W^\pm, G^\pm$, and neutral particles including A, Z, G^0 circulating in the loop.

$$\mathcal{T}^B_{i,\mathrm{Trig}} = \sum_{\phi=h,H}\left(\mathcal{T}^{B,\phi-A}_{i,\mathrm{Trig}} + \mathcal{T}^{B,\phi-H^\pm}_{i,\mathrm{Trig}} + \mathcal{T}^{B,\phi-W^\pm}_{i,\mathrm{Trig}} + \mathcal{T}^{B,\phi-Z}_{i,\mathrm{Trig}} + \mathcal{T}^{B,\phi-W^\pm Z}_{i,\mathrm{Trig}}\right) \tag{A15}$$

Each contribution of $\mathcal{T}^B_{1,\mathrm{Trig}}$ and $\mathcal{T}^B_{2,\mathrm{Trig}}$ is calculated from the corresponding Figs. A1, A2, A3, A4 and A5, respectively. In contrast, the form factor $\mathcal{T}^B_{3,\mathrm{Trig}}$ makes no contribution in one-loop boson-exchanging diagrams. In Fig. A1, the contribution in first for exchanging of ϕ and the pseudo-scalar Higgs A are given as follows.

$$\begin{aligned}\frac{\mathcal{T}^{B,\phi-A}_{1,\mathrm{Trig}}}{g_{AH^-W^+}\cdot g_{\phi AZ}} =& -\frac{g_{\phi W^\pm W^\mp}}{8\pi^2\cdot m_W^2}\left[\left(m_A^2+m_{H^\pm}^2-\xi_W m_W^2\right)C_{00}+2m_{H^\pm}^2 C_{002}+\left(m_{H^\pm}^2-m_W^2+m_Z^2\right)C_{001}\right](Z,W,H^\pm;A,\phi,\xi_W W)\\ &+\frac{g_{\phi W^\pm W^\mp}}{8\pi^2\cdot m_W^2}\left[2m_{H^\pm}^2 C_{00}+\left(m_{H^\pm}^2-m_W^2+m_Z^2\right)C_{001}+2m_{H^\pm}^2 C_{002}\right](Z,W,H^\pm;A,\phi,W)\\ &-\frac{g_{\phi H^\pm H^\mp}}{4\pi^2}C_{00}(Z,H^\pm,W;A,\phi,H^\pm),\end{aligned} \tag{A16}$$

$$\begin{aligned}\frac{\mathcal{T}^{B,\phi-A}_{2,\mathrm{Trig}}}{g_{AH^-W^+}\cdot g_{\phi AZ}} =& \frac{g_{\phi W^\pm W^\mp}}{8\pi^2\cdot m_W^2}\left[2\left(C_{00}+C_{001}\right)+\left(m_{H^\pm}^2-m_W^2+m_Z^2\right)C_{112}+\left(3m_{H^\pm}^2-m_W^2+m_Z^2\right)\left(C_{12}+C_{122}\right)+4\left(m_{H^\pm}^2C_{22}+C_{002}\right)\right.\\ &\left.+2\left(m_{H^\pm}^2-m_W^2\right)C_2+2m_{H^\pm}^2C_{222}\right](Z,W,H^\pm;A,\phi,W)+\frac{g_{\phi W^\pm W^\mp}}{8\pi^2\cdot m_W^2}\left[\left(m_W^2-m_Z^2-3m_{H^\pm}^2\right)C_{122}\right.\\ &-2\left(C_{00}+C_{001}+2C_{002}\right)-\left(m_A^2+m_{H^\pm}^2-\xi_W m_W^2\right)C_2-\left(m_{H^\pm}^2-m_W^2+m_Z^2\right)C_{112}\\ &-\left(m_A^2+2m_{H^\pm}^2-\left(\xi_W+1\right)m_W^2+m_Z^2\right)C_{12}-2m_{H^\pm}^2C_{222}\\ &\left.-\left(m_A^2+3m_{H^\pm}^2-\xi_W m_W^2\right)C_{22}\right](Z,W,H^\pm;A,\phi,\xi_W W)+\frac{g_{\phi H^\pm H^\mp}}{4\pi^2}C_{12}(Z,H^\pm,W;A,\phi,H^\pm),\end{aligned} \tag{A17}$$

$$\frac{\mathcal{T}^{B,\phi-A}_{3,\mathrm{Trig}}}{g_{AH^-W^+}\cdot g_{\phi AZ}} = 0. \tag{A18}$$

Following Fig. A2, the one-loop contributions from the exchange of ϕ and the charged Higgs $H^\pm$ are expressed as follows.

$$\begin{aligned}\frac{\mathcal{T}^{B,\phi-H^\pm}_{1,\mathrm{Trig}}}{16\pi^2\cdot g_{\phi H^\pm H^\mp}} =& \; g_{\phi H^-W^+Z}\cdot B_0(H^\pm;\phi,H^\pm)\\ &-4\,g_{\phi H^-W^+}\cdot g_{ZH^\pm H^\mp}\,C_{00}(W,Z,H^\pm;\phi,H^\pm,H^\pm),\end{aligned} \tag{A19}$$

$$\begin{aligned}\frac{\mathcal{T}^{B,\phi-H^\pm}_{2,\mathrm{Trig}}}{16\pi^2\cdot g_{\phi H^\pm H^\mp}} =& -4g_{\phi H^-W^+}\cdot g_{ZH^\pm H^\mp}\left(C_2+C_{12}+C_{22}\right)\\ &\times(W,Z,H^\pm;\phi,H^\pm,H^\pm),\end{aligned} \tag{A20}$$

$$\frac{\mathcal{T}^{B,\phi-H^\pm}_{3,\mathrm{Trig}}}{16\pi^2\cdot g_{\phi H^\pm H^\mp}} = 0. \tag{A21}$$

From Fig. A3, we obtain the form factors involving the neutral scalar Higgs boson ϕ in association with the vector boson $W^\pm$ and the Goldstone bosons $G^\pm$ in the loop. The factor is given by

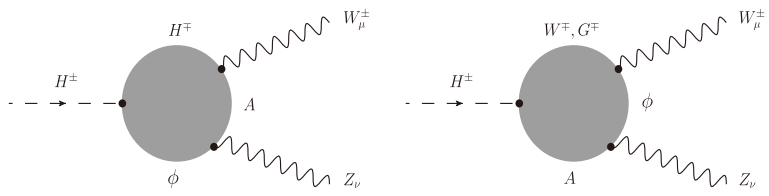

Fig. A1. One-loop triangle Feynman diagrams with $\phi = h,H,A$, together with $H^\pm$ or $W^\pm$ propagating in the loop.

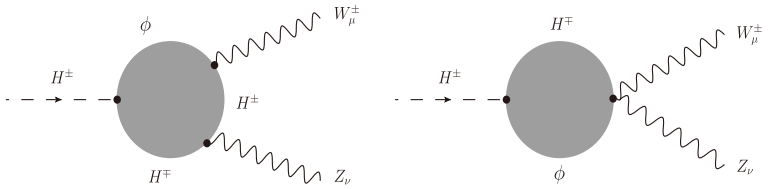

Fig. A2. One-loop triangle Feynman diagrams with $\phi = h, H$ and $H^{\pm}$ in the loop.

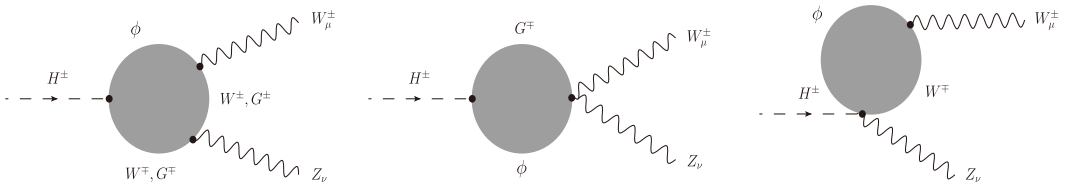

Fig. A3. One-loop triangle diagrams with $\phi = h, H$ and $W^{\pm}$ in the loop.

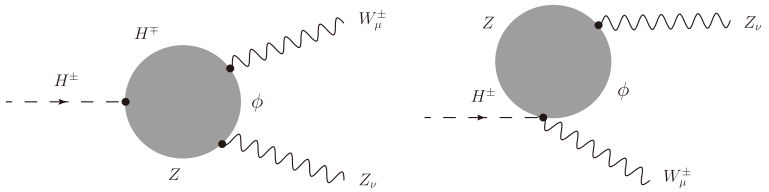

Fig. A4. One-loop triangle diagrams with $\phi = h, H$ and Z as internal lines in the loop.

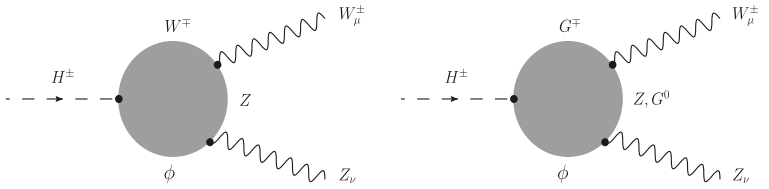

Fig. A5. One-loop triangle Feynman diagrams with $\phi = h, H$ exchanging in association with $W^{\pm}$ and Z contributions in the loop.

$$
\begin{aligned}
\frac{\mathcal{T}^{B,\phi-W^{\pm}}_{1,\mathrm{Trig}}}{g_{\phi W^{\pm}W^{\mp}}} = {} & \frac{g_{\phi H^{-}W^{+}}\cdot g_{ZW^{\pm}W^{\mp}}}{32\pi^{2}\cdot m_{W}^{4}}\Big\{2m_{W}^{2}\Big[A_{0}(W)-A_{0}(\xi_{W}W)\Big]+\Big[2m_{W}^{2}\big(m_{H^{\pm}}^{2}-m_{\phi}^{2}+m_{Z}^{2}-m_{W}^{2}\big)B_{0}-2m_{Z}^{2}B_{00}\Big](Z;W,\xi_{W}W) \\
& +\Big[2m_{W}^{2}\big(m_{\phi}^{2}-m_{H^{\pm}}^{2}-m_{Z}^{2}\big)B_{0}+2\big(m_{Z}^{2}-m_{W}^{2}\big)B_{00}\Big](Z;W,W)+2m_{W}^{2}B_{00}(Z;\xi_{W}W,\xi_{W}W) \\
& -s_{W}^{2}m_{Z}^{2}\big(m_{\phi}^{2}-m_{H^{\pm}}^{2}\big)B_{0}(H^{\pm};\phi,\xi_{W}W)+2m_{W}^{2}\Big[\big(m_{H^{\pm}}^{2}-m_{\phi}^{2}\big)\big(m_{H^{\pm}}^{2}+m_{W}^{2}-m_{Z}^{2}\big)C_{2}+2m_{W}^{2}\big(m_{H^{\pm}}^{2}-m_{\phi}^{2}\big)C_{1} \\
& -m_{\phi}^{2}\big(m_{\phi}^{2}-m_{H^{\pm}}^{2}\big)C_{0}\Big](W,Z,H^{\pm};\phi,W,\xi_{W}W)+2m_{W}^{2}\Big[\big(m_{W}^{2}-m_{H^{\pm}}^{2}-m_{\phi}^{2}\big)C_{00}-\big(m_{H^{\pm}}^{2}+m_{W}^{2}-m_{Z}^{2}\big)C_{002} \\
& -2m_{H^{\pm}}^{2}C_{001}\Big](H^{\pm},Z,W;\phi,W,\xi_{W}W)\Big\}+\frac{g_{\phi H^{-}W^{+}}\cdot g_{ZW^{\pm}W^{\mp}}}{32\pi^{2}\cdot m_{W}^{4}}\Big\{2m_{W}^{2}\Big[\big(m_{H^{\pm}}^{2}+m_{W}^{2}-m_{Z}^{2}\big)C_{001}+2m_{H^{\pm}}^{2}C_{002}\Big] \\
& +2m_{W}^{2}\Big[m_{\phi}^{4}-m_{\phi}^{2}\big(m_{H^{\pm}}^{2}+m_{Z}^{2}\big)-\big(m_{H^{\pm}}^{2}-m_{W}^{2}\big)\big(m_{W}^{2}-m_{Z}^{2}\big)\Big]C_{0}+2\Big[m_{\phi}^{2}\big(m_{Z}^{2}-m_{W}^{2}\big)-m_{Z}^{2}\big(m_{H^{\pm}}^{2}+m_{W}^{2}\big) \\
& +m_{W}^{2}\big(3m_{H^{\pm}}^{2}+m_{W}^{2}\big)\Big]C_{00}+2m_{W}^{4}\big(2m_{\phi}^{2}-m_{H^{\pm}}^{2}-m_{W}^{2}-m_{Z}^{2}\big)C_{1}+2m_{W}^{2}\Big[m_{\phi}^{2}\big(m_{H^{\pm}}^{2}+m_{W}^{2}-m_{Z}^{2}\big) \\
& +m_{H^{\pm}}^{2}\big(m_{Z}^{2}-m_{H^{\pm}}^{2}\big)+m_{W}^{2}\big(m_{Z}^{2}-m_{W}^{2}\big)\Big]C_{2}\Big\}(W,Z,H^{\pm};\phi,W,W) \\
& -\frac{g_{\phi H^{-}W^{+}Z}}{16\pi^{2}\cdot m_{W}^{2}}\Big[\big(m_{W}^{2}B_{0}-B_{00}\big)(W;\phi,W)+B_{00}(W,\phi,\xi_{W}W)\Big],
\end{aligned}
\tag{A22}
$$

$$\begin{aligned}\frac{\mathcal{T}^{B,\phi-W^\pm}_{2,\mathrm{Trig}}}{g_{\phi W^\pm W^\mp}} =& -\frac{g_{\phi H^- W^+}\cdot g_{ZW^\pm W^\mp}}{8\pi^2\cdot m_W^2}\left\{\left(B_0+B_1\right)(Z;W,\xi_W W)+B_1(Z;W,W)\right\}-\frac{g_{\phi H^- W^+}\cdot g_{ZW^\pm W^\mp}}{16\pi^2\cdot m_W^4}\left\{4m_W^4 C_1\right.\\ &+\left[m_W^2\left(3m_\phi^2-m_{H^\pm}^2+m_W^2\right)-m_Z^2\left(m_\phi^2-m_{H^\pm}^2+m_W^2\right)\right]C_2+\left[m_\phi^2\left(m_W^2-m_Z^2\right)+m_{H^\pm}^2\left(m_Z^2-2m_W^2\right)\right]C_{12}\\ &+2m_W^2\left(C_{00}-C_{001}-2C_{002}\right)+\left(m_W^2-m_Z^2\right)\left(m_\phi^2-m_{H^\pm}^2-m_W^2\right)C_{22}-m_W^2\left(m_{H^\pm}^2+m_W^2-m_Z^2\right)C_{112}\\ &\left.+m_W^2\left(m_Z^2-m_W^2-3m_{H^\pm}^2\right)C_{122}-2m_{H^\pm}^2m_W^2C_{222}\right\}(W,Z,H^\pm;\phi,W,W)-\frac{g_{\phi H^- W^+}\cdot g_{ZW^\pm W^\mp}}{16\pi^2\cdot m_W^4}\\ &\times\left\{m_W^2\left(m_W^2-m_\phi^2-m_{H^\pm}^2\right)C_1+m_W^2\left(m_\phi^2-m_{H^\pm}^2-m_W^2\right)C_{11}+m_W^2\left(m_\phi^2-2m_W^2+m_Z^2\right)C_{12}-2m_W^2\left(C_{00}-C_{002}-2C_{001}\right)\right.\\ &\left.+m_W^2\left(m_W^2-m_Z^2+3m_{H^\pm}^2\right)C_{112}+m_W^2\left(m_{H^\pm}^2+m_W^2-m_Z^2\right)C_{122}+2m_{H^\pm}^2m_W^2C_{111}\right\}(H^\pm,Z,W;\phi,W,\xi_W W),\end{aligned}\tag{A23}$$

$$\frac{\mathcal{T}^{B,\phi-W^\pm}_{3,\mathrm{Trig}}}{g_{\phi W^\pm W^\mp}}=0.\tag{A24}$$

As shown in Fig. A4, the corresponding one-loop form factors, with both Higgs bosons ϕ and the vector boson Z exchanged in the loop given as follows.

$$\begin{aligned}\frac{\mathcal{T}^{B,\phi-Z}_{1,\mathrm{Trig}}}{g_{\phi ZZ}} =& -\frac{g_{\phi H^- W^+ Z}}{16\pi^2\cdot m_Z^2}\left[\left(m_Z^2B_0-B_{00}\right)(Z;\phi,Z)\right.\\ &\left.+B_{00}(Z;\phi,\xi_Z Z)\right]-\frac{g_{\phi H^- W^+}\cdot g_{ZH^\pm H^\mp}}{8\pi^2\cdot m_Z^2}\\ &\times\left[B_{00}(Z;\phi,Z)-B_{00}(Z;\phi,\xi_Z Z)\right.\\ &\left.-m_Z^2C_{00}(W,H^\pm,Z;\phi,H^\pm,Z)\right],\end{aligned}\tag{A25}$$

$$\begin{aligned}\frac{\mathcal{T}^{B,\phi-Z}_{2,\mathrm{Trig}}}{g_{\phi ZZ}} =& -\frac{g_{\phi H^- W^+}\cdot g_{ZH^\pm H^\mp}}{16\pi^2}\left(4C_2+2C_{12}\right)\\ &\times(W,H^\pm,Z;\phi,H^\pm,Z),\end{aligned}\tag{A26}$$

$$\frac{\mathcal{T}^{B,\phi-Z}_{3,\mathrm{Trig}}}{g_{\phi ZZ}}=0.\tag{A27}$$

In Fig. A5, the form factors corresponding to the neutral scalar Higgs ϕ accompanied by both the vector bosons $W^\pm$ and Z and the Goldstone bosons $G^\pm$ and G^0 in the loop are represented as follows.

$$\begin{aligned}\frac{\mathcal{T}^{B,\phi-W^\pm Z}_{1,\mathrm{Trig}}}{g_{\phi ZZ}} =& \frac{g_{\phi H^- W^+}\cdot g_{ZW^\pm W^\mp}}{16\pi^2}\xi_W B_0(Z;\phi,Z)+\frac{g_{\phi H^- W^+}\cdot g_{ZW^\pm W^\mp}}{16\pi^2\cdot m_W^2m_Z^2}\left\{\left[c_W^2m_Z^2\left(m_\phi^2-m_{H^\pm}^2\right)\right.\right.\\ &\left.+m_W^2\left(2m_{H^\pm}^2-\xi_W m_W^2\right)\right]C_{00}+m_W^2\left[\left(m_{H^\pm}^2-m_W^2+m_Z^2\right)C_{002}+2m_{H^\pm}^2C_{001}\right]\Big\}(H^\pm,W,Z;\phi,\xi_W W,\xi_Z Z)\\ &+\frac{g_{\phi H^- W^+}\cdot g_{ZW^\pm W^\mp}}{16\pi^2\cdot m_W^2m_Z^2}\left\{m_Z^2\left[m_{H^\pm}^2\left[m_W^2\left(2-3\xi_W\right)+m_Z^2\left(s_W^2-2\right)+2m_{H^\pm}^2\right]-m_\phi^2m_Z^2s_W^2+\xi_W m_W^2\left[m_W^2\left(\xi_W-1\right)+m_Z^2\right]\right]C_0\right.\\ &-m_Z^2\left[m_{H^\pm}^2\left(2m_W^2+2m_Z^2-3m_{H^\pm}^2\right)+2\xi_W m_W^2\left(m_{H^\pm}^2-m_W^2\right)+\left(m_W^2-m_Z^2\right)^2\right]C_1+\left[m_Z^2\left(m_\phi^2s_W^2+2m_W^2-2m_Z^2\right)\right.\\ &\left.-m_{H^\pm}^2\left[2m_W^2+m_Z^2\left(s_W^2-4\right)\right]+\xi_W m_W^2\left(m_W^2-m_Z^2\right)\right]C_{00}-m_Z^2\left[m_{H^\pm}^2\left(2m_W^2+2m_Z^2-3m_{H^\pm}^2\right)+\left(m_W^2-m_Z^2\right)^2\right]C_{12}\\ &+m_Z^2\left[\xi_W m_W^2\left(m_Z^2-m_W^2-3m_{H^\pm}^2\right)+4m_{H^\pm}^2\left(m_{H^\pm}^2+m_W^2-m_Z^2\right)\right]C_2+\left(m_Z^2-m_W^2\right)\left[2m_{H^\pm}^2C_{002}+\left(m_{H^\pm}^2-m_W^2+m_Z^2\right)C_{001}\right]\\ &\left.+m_Z^2\left[\left(m_{H^\pm}^2-m_W^2+m_Z^2\right)\left(m_{H^\pm}^2-m_W^2-m_Z^2\right)C_{11}+2m_{H^\pm}^2\left(m_{H^\pm}^2+m_W^2-m_Z^2\right)C_{22}\right]\right\}(Z,W,H^\pm;\phi,Z,\xi_W W)\\ &+\frac{g_{\phi H^- W^+}\cdot g_{ZW^\pm W^\mp}}{16\pi^2\cdot m_W^2}\times\left\{2\left(m_{H^\pm}^2+m_W^2-m_Z^2\right)\left[\left(m_W^2-m_{H^\pm}^2\right)C_0-C_{00}\right]+\left[m_{H^\pm}^2\left(2m_W^2+2m_Z^2-3m_{H^\pm}^2\right)+\left(m_W^2-m_Z^2\right)^2\right]\right.\\ &\times\left(C_2+C_{12}\right)+\left(m_{H^\pm}^2-m_W^2+m_Z^2\right)\left[\left(m_W^2+m_Z^2-m_{H^\pm}^2\right)C_{22}-C_{002}\right]-2m_{H^\pm}^2\left[\left(m_{H^\pm}^2+m_W^2-m_Z^2\right)\left(2C_1+C_{11}\right)\right.\\ &\left.\left.+\left(C_{00}+C_{001}\right)\right]\right\}\times(H^\pm,W,Z;\phi,W,Z),\end{aligned}\tag{A28}$$

$$\begin{aligned}
\frac{\mathcal{T}^{B,\phi-W^{\pm}Z}_{2,\mathrm{Trig}}}{g_{\phi ZZ}} &= \frac{g_{\phi H^-W^+}\cdot g_{ZW^{\pm}W^{\mp}}}{16\pi^2\cdot m_W^2 m_Z^2}\Big\{\Big[m_Z^2c_W^2\left(m_\phi^2-m_{H^{\pm}}^2\right)+m_W^2\left(2m_{H^{\pm}}^2-\xi_W m_W^2\right)\Big]C_1+\Big[m_Z^2c_W^2\left(m_\phi^2-m_{H^{\pm}}^2\right)+m_W^2\left(4m_{H^{\pm}}^2-\xi_W m_W^2\right)\Big]C_{11}\\
&+\Big[m_Z^2\left(c_W^2m_\phi^2+m_W^2\right)-m_{H^{\pm}}^2\left(c_W^2m_Z^2-3m_W^2\right)-m_W^4\left(\xi_W+1\right)\Big]C_{12}+2m_W^2m_{H^{\pm}}^2C_{111}+m_W^2\left(3m_{H^{\pm}}^2-m_W^2+m_Z^2\right)C_{112}\\
&+m_W^2\left(m_{H^{\pm}}^2-m_W^2+m_Z^2\right)C_{122}+2m_W^2\left(C_{00}+2C_{001}+C_{002}\right)\Big\}(H^{\pm},W,Z;\phi,\xi_WW,\xi_ZZ)\\
&+\frac{g_{\phi H^-W^+}\cdot g_{ZW^{\pm}W^{\mp}}}{16\pi^2\cdot m_W^2m_Z^2}\Big\{\left(m_Z^2-m_W^2\right)\Big[2C_{00}+2C_{001}+4C_{002}+2m_{H^{\pm}}^2C_{222}+\left(m_{H^{\pm}}^2-m_W^2+m_Z^2\right)C_{112}\\
&+\left(3m_{H^{\pm}}^2-m_W^2+m_Z^2\right)C_{122}\Big]+\Big[m_\phi^2m_Z^2s_W^2-m_{H^{\pm}}^2\left(m_W^2-m_Z^2\right)+\xi_Wm_W^2\left(m_W^2-m_Z^2\right)\Big]C_2+\Big[m_\phi^2m_Z^2s_W^2-3m_{H^{\pm}}^2\left(m_W^2-m_Z^2\right)\\
&+\xi_Wm_W^2\left(m_W^2-m_Z^2\right)\Big]C_{22}-\Big[3m_{H^{\pm}}^2m_W^2-m_Z^2\left(m_\phi^2s_W^2+m_Z^2\right)+m_{H^{\pm}}^2m_Z^2\left(s_W^2-3\right)-m_W^4\left(\xi_W+1\right)\\
&+m_W^2m_Z^2\left(\xi_W+2\right)\Big]C_{12}\Big\}(Z,W,H^{\pm};\phi,Z,\xi_WW)+\frac{g_{\phi H^-W^+}\cdot g_{ZW^{\pm}W^{\mp}}}{16\pi^2\cdot m_W^2}\Big\{\left(m_W^2-m_Z^2-3m_{H^{\pm}}^2\right)\left(C_{12}+C_{112}\right)\\
&-\left(m_{H^{\pm}}^2-m_W^2+m_Z^2\right)C_{122}+2m_W^2\left(C_1+2C_2\right)-2m_{H^{\pm}}^2\left(C_1+2C_{11}+C_{111}\right)-2\left(C_{00}\\
&+2C_{001}+C_{002}\right)\Big\}(H^{\pm},W,Z;\phi,W,Z),\\
\frac{\mathcal{T}^{B,\phi-W^{\pm}Z}_{3,\mathrm{Trig}}}{g_{\phi ZZ}} &= 0.
\end{aligned} \tag{A29}$$

Form factors $\mathcal{T}^B_{i,\mathrm{Self}}$:

Following Fig. A6, the form factors $\mathcal{T}^B_{i,\mathrm{Self}}$ for $i=1,2,3$ are decomposed into two contributions from one-point ($1P$) and two-point ($2P$) Feynman diagrams. These factors are expressed as follows.

$$\mathcal{T}^B_{i,\mathrm{Self}}=\mathcal{T}^B_{i,\mathrm{Self}-1P}+\sum_{\phi=h,H}\left(\mathcal{T}^{B,\phi-H^{\pm}}_{i,\mathrm{Self}-2P}+\mathcal{T}^{B,\phi-W^{\pm}}_{i,\mathrm{Self}-2P}\right) \tag{A30}$$

In this equation, the form factors above for $i=1$ are obtained as follows.

$$\begin{aligned}
\frac{\mathcal{T}^B_{1,\mathrm{Self}-1P}}{g_{ZW^{\pm}W^{\mp}}} &= \frac{m_Ws_W^2}{32\pi^2\cdot c_W^2\left(m_{H^{\pm}}^2-\xi m_W^2\right)}\times\Big\{g_{G^0G^0H^-G^+}A_0(\xi_ZZ)+2g_{G^+G^-H^-G^+}A_0(\xi_WW)\\
&+g_{AAH^-G^+}A_0(A)+2g_{H^+H^-H^-G^+}A_0(H^{\pm})+g_{hhH^-G^+}A_0(h)+g_{HHH^-G^+}A_0(H)\Big\},
\end{aligned} \tag{A31}$$

$$\begin{aligned}
\frac{\mathcal{T}^{B,\phi-H^{\pm}}_{1,\mathrm{Self}-2P}}{g_{ZW^{\pm}W^{\mp}}} &= -\frac{g_{\phi H^-W^+}\cdot g_{\phi H^{\pm}H^{\mp}}}{16\pi^2\cdot m_W^2\left(m_{H^{\pm}}^2-\xi_Wm_W^2\right)}\Big\{2\xi_Wm_W^2\left(m_W^2-m_Z^2\right)B_1(H^{\pm};\phi,H^{\pm})\\
&+\Big[m_Z^2s_W^2\left(m_{H^{\pm}}^2-m_\phi^2\right)+\xi_Wm_W^2\left(m_W^2-m_Z^2\right)\Big]B_0(H^{\pm};\phi,H^{\pm})\Big\},
\end{aligned} \tag{A32}$$

$$\begin{aligned}
\frac{\mathcal{T}^{B,\phi-W^{\pm}}_{1,\mathrm{Self}-2P}}{g_{ZW^{\pm}W^{\mp}}} &= -\frac{g_{\phi H^-W^+}\cdot g_{\phi W^{\pm}W^{\mp}}}{32\pi^2\cdot m_W^4\left(m_{H^{\pm}}^2-\xi_Wm_W^2\right)}\times\Big\{s_W^2m_Z^2\Big[\left(m_\phi^2-m_{H^{\pm}}^2\right)A_0(W)-\left(m_\phi^2-m_{H^{\pm}}^2+\xi_Wm_W^2\right)A_0(\xi_WW)\Big]\\
&+\left(m_\phi^2-m_{H^{\pm}}^2\right)\Big[s_W^2m_{H^{\pm}}^2m_Z^2+\xi_Wm_W^2\left(m_W^2-m_Z^2\right)\Big]B_0(H^{\pm};\phi,\xi_WW)+2m_W^2\Big[\xi_W\left(m_W^2-m_Z^2\right)\left(m_{H^{\pm}}^2+m_W^2-m_\phi^2\right)\\
&+s_W^2m_{H^{\pm}}^2m_Z^2\Big]B_1(H^{\pm};\phi,W)+s_W^2m_Z^2\Big[\left(m_\phi^2-m_{H^{\pm}}^2\right)^2-m_W^2\left(m_\phi^2+m_{H^{\pm}}^2\right)\Big]B_0(H^{\pm};\phi,W)\\
&-2\xi_Wm_W^2\left(m_W^2-m_Z^2\right)\left(m_\phi^2-m_{H^{\pm}}^2+m_W^2\right)B_0(H^{\pm};\phi,W)\Big\}.
\end{aligned} \tag{A33}$$

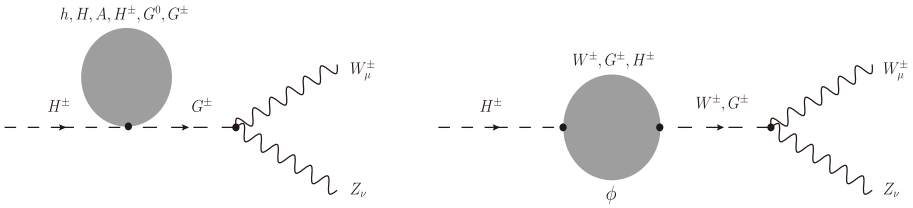

Fig. A6. Self-energy Feynman diagram contributions to the external leg $H^\pm$.

Other values for $i = 2,3$ have no contribution, or

$$\mathcal{T}^{B}_{i,\text{Self}-1P} = \mathcal{T}^{B,\phi-H^\pm}_{i,\text{Self}-2P} = \mathcal{T}^{B,\phi-W^\pm}_{i,\text{Self}-2P} = 0. \tag{A34}$$

Form factors $\mathcal{T}^{B}_{i,\text{Tad}}$*:*

According to Fig. A7, the form factor $\mathcal{T}^{B}_{i,\text{Tad}}$ for $i = 1,2,3$ is expressed in terms of the scalar Higgs $\phi \equiv h, H$ pole coupling with the bubble diagrams. In these loops, the neutral and pseudo-scalar Higgs particles h, H, A, the charged Higgs $H^\pm$, the vector bosons $W^\pm$ and Z, the Goldstone bosons $G^\pm$ and G^0, and the corresponding ghost particles $u_\pm$ and u_Z are all taken into account. As a result, the factor is given by

$$\mathcal{T}^{B}_{i,\text{Tad}} = \sum_{\phi=h,H} \mathcal{T}^{B,\phi}_{i,\text{Tad}}. \tag{A35}$$

where the form factors are expressed as follows.

$$\begin{aligned}
\mathcal{T}^{B,\phi}_{1,\text{Tad}} = & -\frac{1}{64\pi^2 \cdot m_\phi^2 \left(m_{H^\pm}^2 - \xi_W m_W^2\right)} \times \Big[g_{\phi H^- W^+ Z} \left(m_{H^\pm}^2 - \xi_W m_W^2\right) + \left(m_\phi^2 - m_{H^\pm}^2\right) t_W^2 \, g_{\phi H^- W^+} \cdot g_{ZW^\pm W^\mp} \\
& + \xi_W \left(m_Z^2 - m_W^2\right) g_{\phi H^- W^+} \cdot g_{ZW^\pm W^\mp} \Big] \times \Big\{ 4 m_Z^2 \, g_{\phi ZZ} + 8 m_W^2 \, g_{\phi W^\pm W^\mp} + 2 g_{\phi AA} \, A_0(A) + 2 g_{\phi hh} \, A_0(h) \\
& + 2 \, g_{\phi HH} \, A_0(H) + 4 g_{\phi H^\pm H^\mp} \, A_0(H^\pm) - 12 g_{\phi W^\pm W^\mp} A_0(W) - 6 g_{\phi ZZ} \, A_0(Z) - g_{\phi ZZ} \frac{m_\phi^2}{m_Z^2} \, A_0(\xi_Z Z) \\
& - 2 \frac{m_\phi^2}{m_W^2} \, g_{\phi W^\pm W^\mp} \, A_0(\xi_W W) \Big\},
\end{aligned} \tag{A36}$$

$$\mathcal{T}^{B,\phi}_{2,\text{Tad}} = \mathcal{T}^{B,\phi}_{3,\text{Tad}} = 0. \tag{A37}$$

Form factors $\mathcal{T}^{F}_{i,\text{Trig}}$*:*

The form factors $\mathcal{T}^{F}_{i,\text{Trig}}$, for $i = 1,2,3$ as depicted in the corresponding Fig. A8 are given by

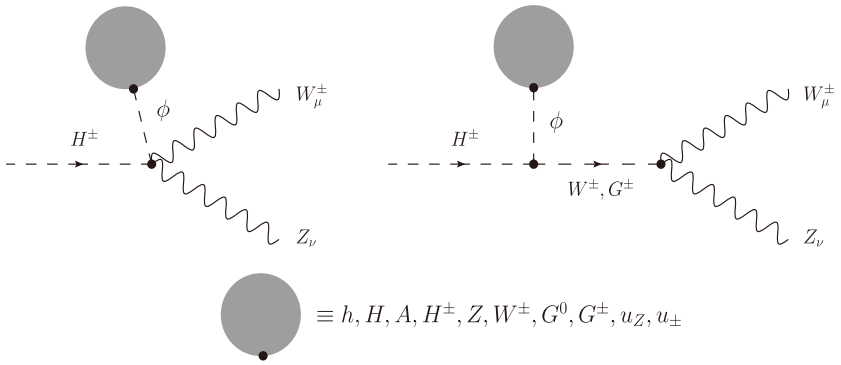

Fig. A7. Tadpole Feynman diagram contributions with poles $\phi \equiv h, H$.

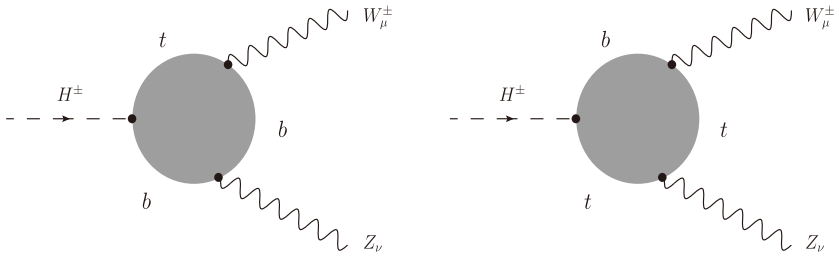

Fig. A8. One-loop triangle Feynman diagrams with fermion loops.

$$\begin{aligned}\frac{\mathcal{T}^{F}_{1,\mathrm{Trig}}}{g_{W^+\bar{t}b}} =& \frac{N^C_Q}{8\pi^2}\cdot\Big\{g^L_{H^-t\bar{b}}m_b^2\left[g^L_{Zt\bar{t}}B_0(Z;t,t)-\left(g^R_{Zb\bar{b}}-g^L_{Zb\bar{b}}\right)B_0(Z;b,b)\right]-g^R_{H^-t\bar{b}}m_t^2\left[\left(g^R_{Zt\bar{t}}-g^L_{Zt\bar{t}}\right)B_0(Z;t,t)-g^L_{Zb\bar{b}}B_0(Z;b,b)\right]\\&-m_t^2m_b^2\left[g^R_{Zt\bar{t}}\cdot g^L_{H^-t\bar{b}}C_0(W,Z,H^{\pm};b,t,t)+g^R_{Zb\bar{b}}\cdot g^R_{H^-t\bar{b}}C_0(Z,H^{\pm},W;b,b,t)\right]\Big\}\\&+\frac{N^C_Q}{16\pi^2}\cdot\Big\{-g^L_{Zb\bar{b}}\cdot g^L_{H^-t\bar{b}}m_b^2\left[2\left(m_W^2-m_t^2\right)C_0+4C_{00}+2m_W^2C_2-\left(m_{H^{\pm}}^2-m_W^2-m_Z^2\right)C_1\right](Z,H^{\pm},W;b,b,t)\\&+g^L_{Zt\bar{t}}\cdot g^L_{H^-t\bar{b}}m_b^2\left[\left(2m_b^2+m_{H^{\pm}}^2+m_W^2-m_Z^2\right)C_0-4C_{00}+\left(m_{H^{\pm}}^2+3m_W^2-m_Z^2\right)C_1+\left(3m_{H^{\pm}}^2+m_W^2-m_Z^2\right)C_2\right]\\&\times(W,Z,H^{\pm};b,t,t)-g^R_{Zb\bar{b}}\cdot g^L_{H^-t\bar{b}}m_b^2\left[\left(2m_t^2-m_{H^{\pm}}^2-m_W^2+m_Z^2\right)C_0+\left(m_{H^{\pm}}^2-m_W^2+m_Z^2\right)C_1\right.\\&\left.-\left(m_{H^{\pm}}^2+m_W^2-m_Z^2\right)C_2\right](Z,H^{\pm},W;b,b,t)-g^L_{Zb\bar{b}}\cdot g^R_{H^-t\bar{b}}m_t^2\left[2\left(m_W^2-m_t^2\right)C_0+4C_{00}-2\left(m_{H^{\pm}}^2-m_W^2\right)C_1\right.\\&\left.+\left(m_{H^{\pm}}^2+3m_W^2-m_Z^2\right)C_2\right](Z,H^{\pm},W;b,b,t)+g^L_{Zt\bar{t}}\cdot g^R_{H^-t\bar{b}}m_t^2\left[2m_b^2C_0-4C_{00}+\left(m_{H^{\pm}}^2+m_W^2-m_Z^2\right)C_2\right.\\&\left.+2m_W^2C_1\right](W,Z,H^{\pm};b,t,t)-g^R_{Zt\bar{t}}\cdot g^R_{H^-t\bar{b}}m_t^2\left[2m_b^2C_0+\left(m_{H^{\pm}}^2+m_W^2-m_Z^2\right)C_1\right.\\&\left.+2m_{H^{\pm}}^2C_2\right](W,Z,H^{\pm};b,t,t)\Big\},\end{aligned}\tag{A38}$$

$$\begin{aligned}\frac{\mathcal{T}^{F}_{2,\mathrm{Trig}}}{g_{W^+\bar{t}b}} =& \frac{N^C_Q}{8\pi^2}\cdot\Big\{-g^L_{Zt\bar{t}}\cdot g^L_{H^-t\bar{b}}m_b^2\times\left(C_0+C_1+3C_2+2C_{12}+2C_{22}\right)(W,Z,H^{\pm};b,t,t)+g^L_{H^-t\bar{b}}m_b^2\\&\times\left[g^L_{Zb\bar{b}}\left(C_1+2C_{12}\right)-g^R_{Zb\bar{b}}\left(C_0+C_1+C_2\right)\right](Z,H^{\pm},W;b,b,t)+g^L_{Zb\bar{b}}\cdot g^R_{H^-t\bar{b}}m_t^2\left(C_2+2C_{12}\right)(Z,H^{\pm},W;b,b,t)\\&+g^R_{H^-t\bar{b}}m_t^2\left[g^R_{Zt\bar{t}}C_1-g^L_{Zt\bar{t}}\left(C_2+2C_{12}+2C_{22}\right)\right](W,Z,H^{\pm};b,t,t)\Big\},\end{aligned}\tag{A39}$$

$$\begin{aligned}\frac{\mathcal{T}^{F}_{3,\mathrm{Trig}}}{g_{W^+\bar{t}b}} =& \frac{N^C_Q}{8\pi^2}\times\Big\{-g^L_{Zt\bar{t}}\cdot g^L_{H^-t\bar{b}}m_b^2\left(C_0+C_1+C_2\right)(W,Z,H^{\pm};b,t,t)+g^L_{H^-t\bar{b}}m_b^2\left[g^L_{Zb\bar{b}}C_1-g^R_{Zb\bar{b}}\left(C_0+C_1+C_2\right)\right](Z,H^{\pm},W;b,b,t)\\&-m_t^2g^R_{H^-t\bar{b}}\left(g^R_{Zt\bar{t}}C_1+g^L_{Zt\bar{t}}C_2\right)(W,Z,H^{\pm};b,t,t)-m_t^2g^R_{H^-t\bar{b}}g^L_{Zb\bar{b}}C_2(Z,H^{\pm},W;b,b,t)\Big]\Big\},\end{aligned}\tag{A40}$$

where the color index N^C_Q for quarks such as top quark t and bottom quark b exchanging in loop has a value of 3. These related general couplings for these vector boson - fermion vertices are expressed with $g^L_{Zf\bar{f}}=e/(s_Wc_W)\times(I^3_f-s^2_WQ_f)$, $g^R_{Zf\bar{f}}=e/(s_Wc_W)\times(-s^2_WQ_f)$ and $g^R_{W^{\pm}f\bar{f}'}=0$, $g^L_{W^{\pm}f\bar{f}'}\equiv g_{W^{\pm}f\bar{f}'}=e/(\sqrt{2}s_W)$.

Form factors $\mathcal{T}^F_{i,\mathrm{Self}}$*:*

The form factors $\mathcal{T}^F_{i,\mathrm{Self}}$ for $i=1,2,3$, which arise from a typical topology in Fig. A9, are presented as follows.

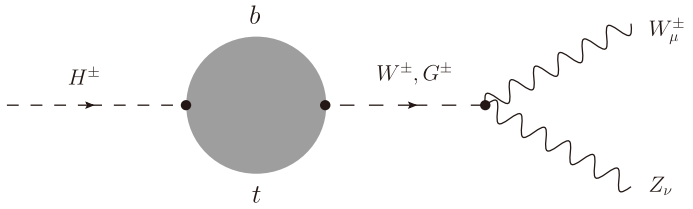

Fig. A9. Self-energy Feynman diagram contributions at the external leg $H^\pm$ with fermion loops.

$$\begin{aligned}\frac{\mathcal{T}^F_{1,\text{Self}}}{g_{ZW^\pm W^\mp}\cdot g_{W^+\bar{t}b}} = \frac{2N^C_Q}{16\pi^2\cdot m_W^2\left(m^2_{H^\pm}-m_W^2\right)}&\left\{s_W^2 m_Z^2\left(m_t^2\, g^R_{H^-t\bar{b}}-m_b^2\, g^L_{H^-t\bar{b}}\right)A_0(b)-g^L_{H^-t\bar{b}}\,m_b^2\left[m_W^2\left(m_Z^2-m_W^2\right)-s_W^2 m^2_{H^\pm}m_Z^2\right]\right.\\
&\times\left(B_0+B_1\right)(H^\pm;b,t)+s_W^2 m_Z^2 m_t^2 g^R_{H^-t\bar{b}}\left(m_t^2-m_b^2-m^2_{H^\pm}\right)B_0(H^\pm;b,t)\\
&\left.+m_t^2 g^R_{H^-t\bar{b}}\left[m_W^2\left(m_W^2-m_Z^2\right)-s_W^2 m^2_{H^\pm}m_Z^2\right]B_1(H^\pm;b,t)\right\},\end{aligned}\tag{A41}$$

$$\mathcal{T}^F_{2,\text{Self}}=\mathcal{T}^F_{3,\text{Self}}=0.\tag{A42}$$

The general couplings involving the Goldstone bosons $G^\pm$ and quarks f, f' exchanging in the loop are given by $\lambda_{G^-f\bar{f}'}=-\mathrm{i}\left(m_{f'}\,g^L_{G^-f\bar{f}'}P_L+m_f\,g^R_{G^-f\bar{f}'}P_R\right)$, and $\lambda_{G^+f'\bar{f}}=-\mathrm{i}\left(m_f\,g^L_{G^+f'\bar{f}}P_L+m_{f'}\,g^R_{G^+f'\bar{f}}P_R\right)$. Furthermore, the left- and right-handed couplings satisfy the relations as $g^L_{G^+f'\bar{f}}=g^R_{G^-f\bar{f}'}=-\frac{1}{m_W}\,g_{W^\pm f\bar{f}'}$ and $g^R_{G^+f'\bar{f}}=g^L_{G^-f\bar{f}'}=+\frac{1}{m_W}\,g_{W^\pm f\bar{f}'}$.

Form factors $\mathcal{T}^F_{i,\text{Tad}}$*:*

Regarding to Fig. A10, form factor $\mathcal{T}^F_{i,\text{Tad}}$ for $i=1,2,3$ is expressed into one-loop contributions by pole $\phi\equiv h,H$ and pole A as follows.

$$\mathcal{T}^F_{i,\text{Tad}}=\mathcal{T}^{F,A}_{i,\text{Tad}}+\sum_{\phi=h,H}\mathcal{T}^{F,\phi}_{i,\text{Tad}}.\tag{A43}$$

where the related general couplings for these scalar Higgs ϕ and pseudo-scalar Higgs A with fermion f vertices are introduced with $g^L_{\phi f\bar{f}}=g^R_{\phi f\bar{f}}\equiv g_{\phi f\bar{f}}$ and $g^R_{Af\bar{f}}=-g^L_{Af\bar{f}}=g_{Af\bar{f}}$ as follows: $-\mathrm{i}m_f\left(g^L_{\phi f\bar{f}}P_L+g^R_{\phi f\bar{f}}P_R\right)=-\mathrm{i}\,m_f\,g_{\phi f\bar{f}}$, and $m_f\left(g^L_{Af\bar{f}}P_L+g^R_{Af\bar{f}}P_R\right)=m_f\,g_{Af\bar{f}}\gamma_5$. Therefore these all form factors at pole A by an analytical relation $g^L_{Af\bar{f}}+g^R_{Af\bar{f}}=0$ and ones for $i=2,3$ at pole ϕ have no contribution for fermion tadpole diagrams,

$$\mathcal{T}^{F,A}_{1,\text{Tad}}=\mathcal{T}^{F,A/\phi}_{2,\text{Tad}}=\mathcal{T}^{F,A/\phi}_{3,\text{Tad}}=0\tag{A44}$$

and thus the remaining form factor that contributes from only pole ϕ is obtained as follows.

$$\begin{aligned}\mathcal{T}^{F,\phi}_{1,\text{Tad}}=&\frac{N^C_Q}{16\pi^2\cdot m_\phi^2\left(m^2_{H^\pm}-m_W^2\right)}\\
&\times\left[\left(m^2_{H^\pm}-m_W^2\right)g_{\phi H^-W^+Z}\right.\\
&+\frac{s_W^2}{c_W^2}\left(m_\phi^2-m^2_{H^\pm}\right)g_{\phi H^-W^+}\cdot g_{ZW^\pm W^\mp}\\
&\left.+\left(m_Z^2-m_W^2\right)g_{\phi H^-W^+}\cdot g_{ZW^\pm W^\mp}\right]\\
&\times\left[4m_b^2\,g_{\phi b\bar{b}}A_0(b)+4m_t^2\,g_{\phi t\bar{t}}A_0(t)\right].\end{aligned}\tag{A45}$$

APPENDIX B: ANALYTICAL CHECKS OF THE ξ-GAUGE INVARIANCE

In this Appendix, we describe the analytical check performed to examine the ξ-gauge invariance of these form factors. Recollect that two gauge parameters ξ_V,

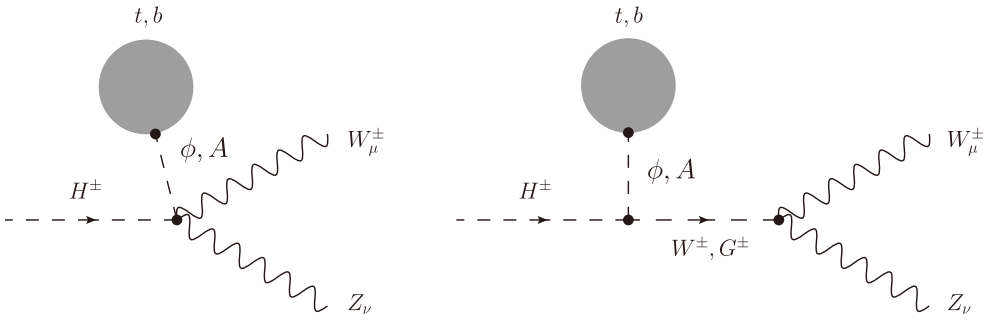

Fig. A10. Tadpole Feynman diagram contributions with poles $\phi\equiv h,H,A$ for fermion loops.

with $V = W,Z$ arise from the propagators of the vector bosons $W^{\pm}$ and Z, the Nambu–Goldstone bosons $G^{\pm}$ and G^0, and the corresponding ghost fields $u_{\pm}$ and u_Z in the general R_ξ gauge. Accordingly, we examine the one-loop form factors $\mathcal{T}_i^B$ $(i = 1,2,3)$ grouped by the bosons exchanged in the loop. In particular, $\mathcal{T}_2^B$ is considered as a representative example for the analytical checks in our simplified demonstration. The one-loop form factor $\mathcal{T}_2^B$ is given as follows.

$$\mathcal{T}_2^B = \mathcal{T}_{2,\mathrm{Trig}}^B + \mathcal{T}_{2,\mathrm{Self}}^B + \mathcal{T}_{2,\mathrm{Tad}}^B. \tag{B1}$$

In this case, the form factors $\mathcal{T}_{2,\mathrm{Self}}^B$ and $\mathcal{T}_{2,\mathrm{Tad}}^B$ do not contribute in the boson-loop group, as explicitly shown in the sections mentioned above [see Eqs. (A34) and (A44)]. As a result, we focus only on the form factor $\mathcal{T}_{2,\mathrm{Trig}}^B$ in Eq. (28), which can be expressed in the concrete form as follows.

$$\mathcal{T}_{2,\mathrm{Trig}}^B = \frac{1}{16\pi^2 \cdot m_{H^\pm}^2 \cdot \Lambda(H^\pm, W, Z)} \times \left(\mathcal{T}_{2,\mathrm{Trig}}^{B,A} + \mathcal{T}_{2,\mathrm{Trig}}^{B,H^\pm} + \mathcal{T}_{2,\mathrm{Trig}}^{B,W^\pm} + \mathcal{T}_{2,\mathrm{Trig}}^{B,Z} + \mathcal{T}_{2,\mathrm{Trig}}^{B,W^\pm Z}\right). \tag{B2}$$

There are five main contributions in which the scalar Higgs ϕ appears together with charged and neutral particles propagating in the loop. These contributions are expressed in terms of the scalar Passarino–Veltman functions A_0, B_0, and C_0. They will be examined explicitly in the following paragraphs for the analytical checks of ξ-gauge invariance.

Next, we consider the remaining form factors $\mathcal{T}_{2,\mathrm{Trig}}^{B,W^\pm}, \mathcal{T}_{2,\mathrm{Trig}}^{B,Z}, \mathcal{T}_{2,\mathrm{Trig}}^{B,W^\pm Z}$, and $\mathcal{T}_{2,\mathrm{Trig}}^{B,A}$, which involve vector and Goldstone boson propagators in terms of the gauge parameters ξ_V for $V = W,Z$. First, we present the representative form for $\mathcal{T}_{2,\mathrm{Trig}}^{B,W^\pm}$ with the cancellation checks of ξ-dependence as follows.

$$\begin{aligned}
\frac{\mathcal{T}_{2,\mathrm{Trig}}^{B,W^\pm}}{g_{ZW^\pm W^\mp}} = \sum_{\phi=h,H} \frac{g_{\phi W^\pm W^\mp} \cdot g_{\phi H^- W^+}}{2c_W^2 m_W^4} \Big\{ & c_{W^\pm}^0 + c_{W^\pm}^1 A_0(\phi) + c_{W^\pm}^2 A_0(W) + c_{W^\pm}^3 B_0(W;\phi,W) + c_{W^\pm}^4 B_0(H^\pm;\phi,W) \\
& + c_{W^\pm}^5 B_0(Z;W,W) + c_{W^\pm}^6 C_0(W,Z,H^\pm;\phi,W,W) + c_{W^\pm}^7 A_0(\xi_W W) + c_{W^\pm}^8 B_0(W;\phi,\xi_W W) + c_{W^\pm}^9 B_0(H^\pm;\phi,\xi_W W) \\
& + c_{W^\pm}^{10} B_0(Z;W,\xi_W W) + c_{W^\pm}^{11} B_0(Z;\xi_W W,\xi_W W) + c_{W^\pm}^{12} C_0(W,Z,H^\pm;\phi,W,\xi_W W) \\
& + c_{W^\pm}^{13} C_0(H^\pm,Z,W;\phi,W,\xi_W W) + c_{W^\pm}^{14} C_0(W,Z,H^\pm;\phi,\xi_W W,\xi_W W) \Big\}.
\end{aligned} \tag{B3}$$

Where the corresponding coefficients in the form factors are listed as follows.

$$\begin{aligned}
c_{W^\pm}^0 &= c_{2W} m_{H^\pm}^2 m_W^2 (m_\phi^2 - m_{H^\pm}^2 - m_W^2)(m_{H^\pm}^2 - m_W^2 - m_Z^2) \cdot \Lambda(H^\pm, W, Z), \\
c_{W^\pm}^1 &= c_{2W} m_W^2 (m_\phi^2 - m_{H^\pm}^2 - m_W^2)(m_{H^\pm}^2 - m_W^2 + m_Z^2) \cdot \Lambda(H^\pm, W, Z), \\
c_{W^\pm}^2 &= -c_W^2 (2m_W^2 - m_Z^2)(m_\phi^2 - m_{H^\pm}^2 - m_W^2)(m_{H^\pm}^2 - m_W^2 + m_Z^2) \cdot \Lambda(H^\pm, W, Z), \\
c_{W^\pm}^3 &= c_W^2 m_{H^\pm}^2 m_\phi^4 (2m_W^2 - m_Z^2)\left[\left(m_{H^\pm}^2 - m_W^2 - m_Z^2\right)^2 + 8m_W^2 m_Z^2\right] - c_W^2 m_{H^\pm}^2 m_\phi^2 (2m_W^2 - m_Z^2)\Big[-2m_Z^2\left(m_{H^\pm}^4 - 5m_{H^\pm}^2 m_W^2 - 12m_W^4\right) \\
&\quad + m_Z^4 (m_{H^\pm}^2 - 3m_W^2) + (m_{H^\pm}^2 + 3m_W^2)(m_{H^\pm}^2 - m_W^2)^2\Big] + 2c_W^2 m_{H^\pm}^2 m_W^2 \Big[-m_Z^4\left(m_{H^\pm}^4 + 16m_{H^\pm}^2 m_W^2 + 7m_W^4\right) \\
&\quad + m_Z^2 (m_{H^\pm}^2 + m_W^2)\left(-m_{H^\pm}^4 + 12m_{H^\pm}^2 m_W^2 + 5m_W^4\right) + 2m_Z^6 (m_{H^\pm}^2 + m_W^2) - 2m_W^2 (m_{H^\pm}^2 - m_W^2)^2 (m_{H^\pm}^2 - 3m_W^2)\Big] \\
&\quad - 6m_{H^\pm}^2 m_W^4 \xi_W \left[c_W^2 (m_W^2 - m_Z^2) + m_W^2 s_W^2\right](m_\phi^2 - m_{H^\pm}^2)(m_{H^\pm}^2 - m_W^2 - m_Z^2),
\end{aligned}$$

$$\begin{aligned}
c_{W^\pm}^4 &= c_W^2 m_\phi^4 (m_Z^2 - 2m_W^2)\left[2m_{H^\pm}^6 + m_{H^\pm}^4 (3m_Z^2 - 5m_W^2) + 2m_{H^\pm}^2 (m_W^2 - m_Z^2)(2m_W^2 + 3m_Z^2) - (m_W^2 - m_Z^2)^3\right] \\
&\quad + 2c_W^2 m_\phi^2 (2m_W^2 - m_Z^2)\left[m_{H^\pm}^8 + 2m_{H^\pm}^6 m_Z^2 - 4m_{H^\pm}^4 (m_W^2 - m_Z^2)^2 + m_{H^\pm}^2\left(4m_W^6 + 3m_W^4 m_Z^2 - 8m_W^2 m_Z^4 + m_Z^6\right)\right. \\
&\quad \left. - m_W^2 (m_W^2 - m_Z^2)^3\right] + c_W^2 m_{H^\pm}^8\left(2m_W^4 + 5m_W^2 m_Z^2 + m_Z^4\right) - 2c_W^2 m_{H^\pm}^6\left(8m_W^6 + 20m_W^4 m_Z^2 - 2m_W^2 m_Z^4 + m_Z^6\right) \\
&\quad + c_W^2 m_{H^\pm}^4\left(28m_W^8 - 46m_W^6 m_Z^2 + 14m_W^4 m_Z^4 + m_W^2 m_Z^6 + m_Z^8\right) + c_W^2 m_W^2 (m_W^2 - m_Z^2)(2m_W^2 - m_Z^2) \\
&\quad \times \left[m_W^2 (m_W^2 - m_Z^2)^2 - 2m_{H^\pm}^2 (4m_W^4 + m_Z^4)\right] - 2m_{H^\pm}^2 m_W^2 (m_\phi^2 - m_{H^\pm}^2 - m_W^2)\xi_W \left[c_W^2 (m_W^2 - m_Z^2) + m_W^2 s_W^2\right] \\
&\quad \times \left[2m_{H^\pm}^4 - m_{H^\pm}^2 (m_W^2 + m_Z^2) - (m_W^2 - m_Z^2)^2\right],
\end{aligned} \tag{B4}$$

$$\frac{c^5_{W^\pm}}{m^2_{H^\pm}m^2_W} = 6m^4_\phi(2m^2_W-m^2_Z)(m^2_{H^\pm}-m^2_W-m^2_Z)+m^2_\phi(2m^2_W-m^2_Z)\times\Big[m^2_{H^\pm}\left(8m^2_Z-10m^2_W-7m^2_{H^\pm}\right)$$
$$+m^2_W\left(17m^2_W+8m^2_Z\right)-m^4_Z\Big]+m^4_{H^\pm}\Big[\left(18m^4_W-3m^2_Wm^2_Z+2m^4_Z\right)-m^2_{H^\pm}(2m^2_W+m^2_Z)\Big]$$
$$+m^2_{H^\pm}\Big[m^2_W\left(18m^4_W+17m^2_Wm^2_Z-6m^4_Z\right)-m^6_Z\Big]+m^2_W\Big[m^2_W\left(35m^2_Wm^2_Z-34m^4_W-16m^4_Z\right)+3m^6_Z\Big], \tag{B5}$$

$$\frac{c^6_{W^\pm}}{2c^2_Wm^2_{H^\pm}} = 3m^6_\phi m^2_Z(2m^2_W-m^2_Z)(m^2_{H^\pm}-m^2_W-m^2_Z)+m^4_\phi m^2_Z(2m^2_W-m^2_Z)\times\Big[m^2_{H^\pm}\left(7m^2_Z-8m^2_W-5m^2_{H^\pm}\right)$$
$$+m^2_W\left(13m^2_W+7m^2_Z\right)-2m^4_Z\Big]+m^2_\phi\Big[m^6_{H^\pm}\left(2m^4_W+m^2_Wm^2_Z-2m^4_Z\right)$$
$$+m^4_{H^\pm}\left(-6m^6_W+23m^4_Wm^2_Z-13m^2_Wm^4_Z+4m^6_Z\right)+m^2_{H^\pm}\left(6m^8_W+15m^6_Wm^2_Z-12m^4_Wm^4_Z+8m^2_Wm^6_Z-2m^8_Z\right)$$
$$-m^4_W\left(2m^6_W+39m^4_Wm^2_Z-27m^2_Wm^4_Z+4m^6_Z\right)\Big]+m^2_W(m^2_{H^\pm}-m^2_W)$$
$$\times\Big[m^6_{H^\pm}(2m^2_W+m^2_Z)+m^4_{H^\pm}\left(-10m^4_W-11m^2_Wm^2_Z+m^4_Z\right)+m^2_{H^\pm}\left(14m^6_W-17m^4_Wm^2_Z+16m^2_Wm^4_Z-2m^6_Z\right)$$
$$-m^2_W\left(6m^6_W+5m^4_Wm^2_Z-7m^2_Wm^4_Z+2m^6_Z\right)\Big],$$
$$c^7_{W^\pm} = -2m^2_{H^\pm}m^2_W\left[c^2_W(m^2_W-m^2_Z)+m^2_Ws^2_W\right]\Lambda(H^\pm,W,Z)=0, \tag{B6}$$

$$\frac{c^8_{W^\pm}}{m^2_{H^\pm}m^2_W} = \left[c^2_W(m^2_W-m^2_Z)+m^2_Ws^2_W\right]\times\Big\{\Big[m^2_\phi m^2_{H^\pm}\left[m^2_{H^\pm}-2m^2_W(4-3\xi_W)-2m^2_Z\right]+2m^2_Wm^2_Zm^2_\phi(8-3\xi_W)$$
$$+m^4_W\,m^2_\phi(7-6\xi_W)+m^4_Z\,m^2_\phi\Big]+m^2_Wm^2_\phi\Big[-m^4_{H^\pm}(7\xi_W+3)+2m^2_{H^\pm}\Big[m^2_W(\xi_W+9)$$
$$+m^2_Z(4\xi_W+3)\Big]-5m^4_W(3-\xi_W)+m^2_Wm^2_Z(6-4\xi_W)-m^4_Z(\xi_W+3)\Big]\Big\}=0, \tag{B7}$$

$$c^9_{W^\pm} = 2\left[c^2_W(m^2_W-m^2_Z)+m^2_Ws^2_W\right](\xi_W-1)\times m^2_{H^\pm}m^2_W(m^2_\phi-m^2_{H^\pm})\left[m^2_{H^\pm}\left(2m^2_{H^\pm}-m^2_W-m^2_Z\right)-(m^2_W-m^2_Z)^2\right]=0, \tag{B8}$$

$$\frac{c^{10}_{W^\pm}}{m^2_{H^\pm}} = \left[c^2_W(m^2_W-m^2_Z)+m^2_Ws^2_W\right]\times\Big\{4m^2_\phi m^2_Z\Big[3m^2_\phi(m^2_Z-m^2_{H^\pm}+m^2_W)-m^2_Z(4m^2_{H^\pm}+m^2_W)\Big]$$
$$+2m^2_\phi m^2_Z\Big[(m^2_{H^\pm}-m^2_W)(7m^2_{H^\pm}+11m^2_W)+m^4_Z\Big]-2m^6_{H^\pm}m^2_Z+m^2_{H^\pm}m^2_Wm^2_Z\left(2m^2_W-3m^2_{H^\pm}\right)$$
$$+m^4_Z\left(2m^2_{H^\pm}+m^2_W\right)\left(2m^2_{H^\pm}-7m^2_W\right)-m^2_W\left(m^2_{H^\pm}-m^2_W\right)^2\left(4m^2_{H^\pm}-5m^2_W\right)+m^2_Z\left(11m^6_W-2m^2_{H^\pm}m^4_Z+3m^2_Wm^4_Z\right)\Big\}$$
$$-\xi_Wm^2_W\Big\{-2m^2_{H^\pm}\Big[3m^2_Z(m^2_\phi+m^2_Z)+m^2_W(m^2_W+m^2_Z)\Big]+m^2_Wm^2_Z(6m^2_\phi-5m^2_Z)$$
$$+6m^2_\phi m^4_Z+m^4_{H^\pm}(m^2_W+6m^2_Z)+m^4_W(m^2_W+4m^2_Z)\Big\}=0, \tag{B9}$$

$$c^{11}_{W^\pm} = \left[c^2_W(m^2_W-m^2_Z)+m^2_Ws^2_W\right]m^2_{H^\pm}m^2_Z(m^2_{H^\pm}-m^2_\phi)\times\Big[6(m^2_\phi-m^2_W\xi_W)(-m^2_{H^\pm}+m^2_W+m^2_Z)-5m^4_W$$
$$+m^2_{H^\pm}(m^2_{H^\pm}+4m^2_W-2m^2_Z)+m^2_Z(4m^2_W+m^2_Z)\Big]=0, \tag{B10}$$

$$\begin{aligned}\frac{c^{12}_{W^\pm}}{2m^2_{H^\pm}} =& \left[c^2_W(m^2_W-m^2_Z)+m^2_W s^2_W\right]\Big\{3m^6_\phi m^2_Z\left(m^2_W+m^2_Z-m^2_{H^\pm}\right)+m^4_\phi\Big[m^4_{H^\pm}(2m^2_W+5m^2_Z)+m^2_{H^\pm}\left(-4m^4_W+m^2_W m^2_Z-7m^4_Z\right)\\&+2(m^2_W-m^2_Z)^2(m^2_W+m^2_Z)\Big]-m^2_\phi m^2_{H^\pm}\Big[m^4_{H^\pm}(3m^2_W+2m^2_Z)+m^2_{H^\pm}\left(-3m^4_W+5m^2_W m^2_Z-4m^4_Z\right)+2m^2_Z(m^2_W-m^2_Z)^2\Big]\\&+m^4_{H^\pm}m^2_W\Big[m^4_{H^\pm}+m^2_{H^\pm}(m^2_W+m^2_Z)-2(m^2_W-m^2_Z)^2\Big]\Big\}-(2\xi_W)m^2_W(m^2_\phi-m^2_{H^\pm})\times\\&\times\Big\{m^2_\phi\Big[m^4_{H^\pm}-2m^2_{H^\pm}(m^2_W+m^2_Z)+m^2_W(m^2_W+4m^2_Z)+m^4_Z\Big]\\&+m^2_W\Big[m^2_{H^\pm}(m^2_W+m^2_Z-2m^2_{H^\pm})+(m^2_W-m^2_Z)^2\Big]\Big\}=0,\end{aligned} \tag{B11}$$

$$\begin{aligned}\frac{c^{13}_{W^\pm}}{2m^2_{H^\pm}} =& \left[c^2_W(m^2_W-m^2_Z)+m^2_W s^2_W\right]\Big\{3m^6_\phi m^2_Z\left(-m^2_{H^\pm}+m^2_W+m^2_Z\right)+m^4_\phi\Big[m^4_{H^\pm}(5m^2_Z-2m^2_W)+m^2_{H^\pm}\left(4m^4_W+6m^2_W m^2_Z-7m^4_Z\right)\\&+2m^6_Z-2m^6_W-3m^2_W m^2_Z(5m^2_W+m^2_Z)\Big]+m^2_\phi\Big[m^4_{H^\pm}\left(6m^4_W-4m^2_W m^2_Z+4m^4_Z-2m^2_{H^\pm}m^2_Z\right)\\&-m^2_{H^\pm}\left(15m^6_W-5m^4_W m^2_Z+m^2_W m^4_Z+2m^6_Z\right)+m^2_W\left(9m^6_W+16m^4_W m^2_Z-8m^2_W m^4_Z+m^6_Z\right)\Big]\\&-m^2_W\Big[m^4_{H^\pm}\left(5m^4_W+3m^2_W m^2_Z+m^4_Z-2m^2_{H^\pm}m^2_Z\right)+m^2_{H^\pm}\left(-16m^6_W+5m^4_W m^2_Z-3m^2_W m^4_Z+m^6_Z\right)\\&+m^2_W\left(11m^6_W-8m^4_W m^2_Z+4m^2_W m^4_Z-m^6_Z\right)\Big]+\xi_W m^2_W\Big[2m^4_\phi\Big[m^2_Z(m^2_{H^\pm}+m^2_W-2m^2_Z)+(m^2_{H^\pm}-m^2_W)^2\Big]\\&-m^2_\phi\Big[m^4_{H^\pm}(m^2_Z-5m^2_W+3m^2_{H^\pm})+m^2_{H^\pm}\left(-5m^+_W 14m^2_W m^2_Z-5m^4_Z\right)+(m^2_W-m^2_Z)(7m^2_W-m^2_Z)(m^2_W+m^2_Z)\Big]\\&-m^2_Z(m^2_{H^\pm}-3m^2_W)(m^4_{H^\pm}-3m^4_W)+m^4_{H^\pm}(m^4_{H^\pm}-8m^4_W)+m^6_Z(m^2_{H^\pm}-m^2_W)-m^4_Z(m^2_{H^\pm}-3m^2_W)(m^2_{H^\pm}+m^2_W)+7m^8_W\Big\}=0,\end{aligned} \tag{B12}$$

$$\begin{aligned}\frac{c^{14}_{W^\pm}}{2m^2_{H^\pm}} =& \left[c^2_W(m^2_W-m^2_Z)+m^2_W s^2_W\right]\times\Big\{m^2_Z(m^2_\phi-m^2_{H^\pm})\Big[3m^4_\phi\left(m^2_{H^\pm}-m^2_W-m^2_Z\right)-2m^2_\phi\Big[m^2_{H^\pm}(m^2_{H^\pm}+m^2_W-2m^2_Z)\\&-2m^4_W+m^2_Z(m^2_W+m^2_Z)\Big]-m^2_W\Big[m^2_{H^\pm}(m^2_W+m^2_Z-2m^2_{H^\pm})+(m^2_W-m^2_Z)^2\Big]\Big]-(\xi_W)m^2_W(m^2_\phi-m^2_{H^\pm})\\&\times\Big[m^4_Z\left(-6m^2_\phi+m^2_{H^\pm}-3m^2_W-m^2_Z\right)+m^2_Z(m^2_{H^\pm}-m^2_W)(6m^2_\phi+m^2_{H^\pm}-3m^2_W)-(m^2_{H^\pm}-m^2_W)^3\Big]\Big\}=0.\end{aligned}$$

We note that the kinematical function is defined as $\Lambda(H^\pm,W,Z)=(m^2_{H^\pm}-m^2_W-m^2_Z)^2-4m^2_W m^2_Z$. Because $c^2_W(m^2_W-m^2_Z)+m^2_W s^2_W=0$, the coefficients $c^7_{W^\pm}=c^8_{W^\pm}=\cdots=c^{14}_{W^\pm}=0$. While $c^3_{W^\pm}$ and $c^4_{W^\pm}$ are independent of ξ, the remaining coefficients $c^{1,2}_{W^\pm}$ and $c^{5,6}_{W^\pm}$ also do not depend on ξ. Consequently, the form factor $\mathcal{T}^B_{2,\mathrm{Trig}}$ becomes ξ-independent. Other form factors are confirmed using the same procedure, which demonstrates that they are also ξ-independent.

APPENDIX C: FEYNMAN DIAGRAMS FOR $H^\pm\to W^\pm Z$ IN THE GENERAL R_ξ

A complete set of one-loop Feynman diagrams relevant to the decay process $H^\pm\to W^\pm Z$ in the general R_ξ gauge is provided in the Appendix.

APPENDIX D: FEYNMAN DIAGRAMS FOR $\mu^+\mu^-\to H^+H^-$ AND $\gamma\gamma\to H^+H^-$ IN THDM

Feynman diagrams for $\mu^+\mu^-\to H^+H^-$ and $\gamma\gamma\to H^+H^-$ in THDM are presented in this appendix. The Feynman diagrams were generated using `FeynArt` [61].

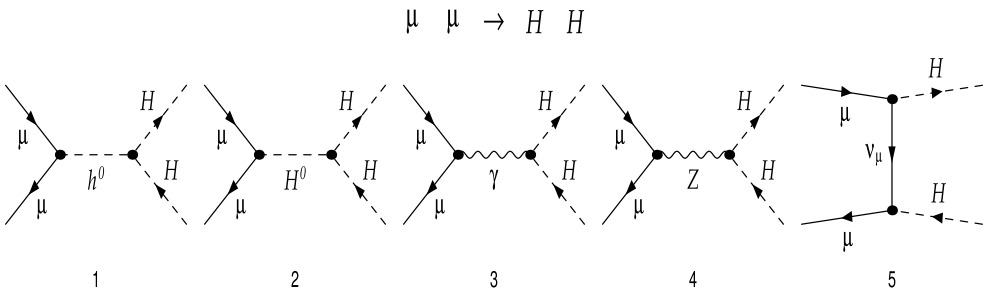

Fig. D1. Feynman diagrams for $\mu^+\mu^- \to H^+H^-$ are generated by `FeynArts` [61].

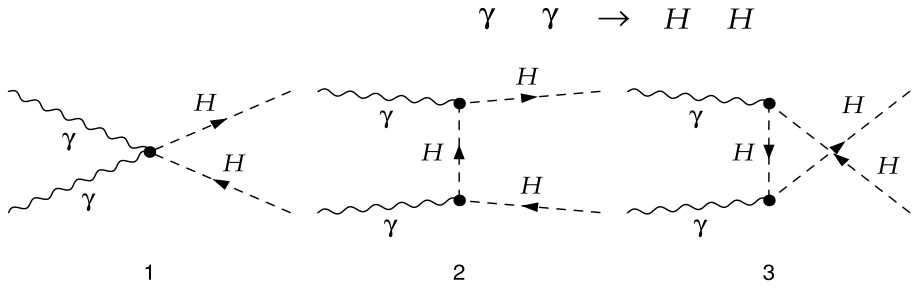

Fig. D2. Feynman diagrams for $\mu^+\mu^- \to H^+H^-$ generated with `FeynArts` [61].

References

[1] S. Chatrchyan *et al.* (CMS), JHEP **07**, 143 (2012), arXiv: 1205.5736[hep-ex]

[2] V. Khachatryan *et al.* (CMS), JHEP **11**, 018 (2015), arXiv: 1508.07774[hep-ex]

[3] G. Aad *et al.* (ATLAS), JHEP **09**, 004 (2023), arXiv: 2302.11739[hep-ex]

[4] G. Aad *et al.* (ATLAS), Eur. Phys. J. C **85**(2), 153 (2025), arXiv: 2407.10096[hep-ex]

[5] G. Aad *et al.* (ATLAS), JHEP **06**, 039 (2012), arXiv: 1204.2760[hep-ex]

[6] G. Aad *et al.* (ATLAS), Eur. Phys. J. C **73**(6), 2465 (2013), arXiv: 1302.3694[hep-ex]

[7] G. Aad *et al.* (ATLAS), JHEP **03**, 127 (2016), arXiv: 1512.03704[hep-ex]

[8] G. Aad *et al.* (ATLAS), JHEP **06**, 145 (2021), arXiv: 2102.10076[hep-ex]

[9] A. M. Sirunyan *et al.* (CMS), JHEP **07**, 126 (2020), arXiv: 2001.07763[hep-ex]

[10] G. Aad *et al.* (ATLAS), Phys. Rev. Lett. **114**(23), 231801 (2015), arXiv: 1503.04233[hep-ex]

[11] M. Aaboud *et al.* (ATLAS), Phys. Lett. B **787**, 68 (2018), arXiv: 1806.01532[hep-ex]

[12] A. M. Sirunyan *et al.* (CMS), Eur. Phys. J. C **81**(8), 723 (2021), arXiv: 2104.04762[hep-ex]

[13] A. M. Sirunyan *et al.* (CMS), JHEP **11**, 115 (2018), arXiv: 1808.06575[hep-ex]

[14] A. M. Sirunyan *et al.* (CMS), Phys. Rev. D **102**(7), 072001 (2020), arXiv: 2005.08900[hep-ex]

[15] A. Tumasyan *et al.* (CMS), JHEP **09**, 032 (2023), arXiv: 2207.01046[hep-ex]

[16] G. Aad *et al.* (ATLAS), JHEP **02**, 143 (2025), arXiv: 2411.03969[hep-ex]

[17] M. Aaboud *et al.* (ATLAS), JHEP **09**, 139 (2018), arXiv: 1807.07915[hep-ex]

[18] G. Aad *et al.* (ATLAS), Phys. Rev. D **111**(7), 072006 (2025), arXiv: 2412.17584[hep-ex]

[19] A. M. Sirunyan *et al.* (CMS), JHEP **07**, 142 (2019), arXiv: 1903.04560[hep-ex]

[20] A. Arhrib, R. Benbrik, S. Moretti *et al.*, Phys. Rev. D **97**(7), 075037 (2018), arXiv: 1712.05018[hep-ph]

[21] A. Arhrib, A. Jueid, and S. Moretti, Phys. Rev. D **98**(11), 115006 (2018), arXiv: 1807.11306[hep-ph]

[22] A. Arhrib, D. Azevedo, R. Benbrik *et al.*, JHEP **10**, 209 (2020), arXiv: 1905.02635[hep-ph]

[23] A. Arhrib, K. Cheung, and C. T. Lu, Phys. Rev. D **102**(9), 095026 (2020), arXiv: 1910.02571[hep-ph]

[24] A. Arhrib, R. Benbrik, H. Harouiz *et al.*, Phys. Rev. D **102**(11), 115040 (2020), arXiv: 2003.11108[hep-ph]

[25] A. Arhrib, R. Benbrik, M. Krab *et al.*, JHEP **10**, 073 (2021), arXiv: 2106.13656[hep-ph]

[26] Y. Wang, A. Arhrib, R. Benbrik *et al.*, JHEP **12**, 021 (2021), arXiv: 2107.01451[hep-ph]

[27] M. Krab, M. Ouchemhou, A. Arhrib *et al.*, Phys. Lett. B **839**, 137705 (2023), arXiv: 2210.09416[hep-ph]

[28] A. Arhrib, M. Krab, and S. Semlali, J. Phys. G **51**(11), 115003 (2024), arXiv: 2402.03195[hep-ph]

[29] A. Arhrib, R. Benbrik, M. Berrouj *et al.*, Phys. Rev. D **111**(9), 095026 (2025), arXiv: 2407.01348[hep-ph]

[30] R. Benbrik, M. Berrouj, M. Boukidi *et al.*, Phys. Lett. B **843**, 138024 (2023)

[31] A. Arhrib, R. Benbrik, M. Boukidi *et al.*, Eur. Phys. J. C **85**(1), 2 (2025), arXiv: 2401.16219[hep-ph]

[32] A. Arhrib, R. Benbrik, M. Boukidi *et al.*, Eur. Phys. J. C **84**(10), 1008 (2024), arXiv: 2403.13021[hep-ph]

[33] R. Benbrik, M. Berrouj, and M. Boukidi, Phys. Rev. D

111(1), 015027 (2025), arXiv: 2408.15985[hep-ph]
[34] R. Benbrik, M. Berrouj, M. Boukidi *et al*., Eur. Phys. J. C **85**(5), 500 (2025)
[35] H. E. Logan and Y. Wu, JHEP **11**, 121 (2018), arXiv: 1809.09127[hep-ph]
[36] B. A. Ouazghour, A. Arhrib, K. Cheung *et al*., Phys. Rev. D **109**(11), 115009 (2024), arXiv: 2308.15664[hep-ph]
[37] B. A. Ouazghour, A. Arhrib, K. Cheung *et al*., Phys. Rev. D **110**(9), 095026 (2024), arXiv: 2408.13952[hep-ph]
[38] B. A. Ouazghour, A. Arhrib, K. Cheung *et al*., arXiv: 2506.01554 [hep-ph]
[39] B. Ait-Ouazghour, A. Arhrib, M. Chabab *et al*., arXiv: 2508.04493[hep-ph]
[40] I. Ahmed, A. Quddus, J. Muhammad *et al*., Chin. Phys. C **49**(4), 043101 (2025), arXiv: 2403.20293[hep-ph]
[41] M. Hashemi and L. Roushandel, Eur. Phys. J. C **84**(9), 966 (2024), arXiv: 2310.06519[hep-ph]
[42] P. Bredt, T. Banno, M. Höfer *et al*., arXiv: 2509.05421[hep-ph]
[43] A. Costantini, F. De Lillo, F. Maltoni *et al*., JHEP **09**, 080 (2020), arXiv: 2005.10289[hep-ph]
[44] R. Capdevilla, D. Curtin, Y. Kahn *et al*., Phys. Rev. D **105**(1), 015028 (2022), arXiv: 2101.10334[hep-ph]
[45] A. Arhrib, R. Benbrik, and M. Chabab, J. Phys. G **34**, 907 (2007), arXiv: 0607182[hep-ph]
[46] S. Kanemura, Phys. Rev. D **61**, 095001 (2000), arXiv: hep-ph/9710237[hep-ph]
[47] S. Kanemura and Y. Mura, JHEP **10**, 041 (2024), arXiv: 2408.06863[hep-ph]
[48] M. Aiko, S. Kanemura, and K. Sakurai, Nucl. Phys. B **973**, 115581 (2021), arXiv: 2108.11868[hep-ph]
[49] J. Hernandez-Sanchez, M. A. Perez, G. Tavares-Velasco *et al*., Phys. Rev. D **69**, 095008 (2004), arXiv: 0402284 [hep-ph]
[50] J. E. Barradas Guevara, F. C. Cazarez Bush, A. Cordero Cid *et al*., J. Phys. G **37**, 115008 (2010), arXiv: 1002.2626[hep-ph]
[51] J. Haller, A. Hoecker, R. Kogler *et al*., Eur. Phys. J. C **78**(8), 675 (2018), arXiv: 1803.01853[hep-ph]
[52] D. T. Tran, Q. H. M. Pham, K. N. T. Ho *et al*., arXiv: 2509.08417 [hep-ph]
[53] G. C. Branco, P. M. Ferreira, L. Lavoura *et al*., Phys. Rept. **516**, 1 (2012), arXiv: 1106.0034[hep-ph]
[54] M. Aoki, S. Kanemura, K. Tsumura *et al*., Phys. Rev. D **80**, 015017 (2009), arXiv: 0902.4665[hep-ph]
[55] P. Bechtle, D. Dercks, S. Heinemeyer *et al*., Eur. Phys. J. C **80**(12), 1211 (2020), arXiv: 2006.06007[hep-ph]
[56] P. Bechtle, S. Heinemeyer, T. Klingl *et al*., Eur. Phys. J. C **81**(2), 145 (2021), arXiv: 2012.09197[hep-ph]
[57] D. Eriksson, J. Rathsman, and O. Stal, Comput. Phys. Commun. **181**, 189 (2010), arXiv: 0902.0851[hep-ph]
[58] F. Mahmoudi, Comput. Phys. Commun. **180**, 1579 (2009), arXiv: 0808.3144[hep-ph]
[59] A. Denner, Fortsch. Phys. **41**, 307 (1993), arXiv: 0709.1075[hep-ph]
[60] S. Navas *et al*. (Particle Data Group), Phys. Rev. D **110**(3), 030001 (2024)
[61] T. Hahn, Comput. Phys. Commun. **140**, 418 (2001), arXiv: 0012260[hep-ph]
[62] M. Cacciari, A. Deandrea, G. Montagna *et al*., EPL **17**, 123 (1992)
[63] M. Skrzypek and S. Jadach, Z. Phys. C **49**, 577 (1991)
[64] M. Skrzypek, Acta Phys. Polon. B **23**, 135 (1992)
[65] G. Belanger, F. Boudjema, J. Fujimoto *et al*., Phys. Rept. **430**, 117 (2006), arXiv: 0308080[hep-ph]
[66] J. H. Kuhn, A. A. Penin, and V. A. Smirnov, Eur. Phys. J. C **17**, 97 (2000), arXiv: 9912503[hep-ph]
[67] A. F. Zarnecki, Acta Phys. Polon. B **34**, 2741 (2003)
[68] M. Chiesa, B. Mele, and F. Piccinini, Eur. Phys. J. C **84**(5), 543 (2024), arXiv: 2109.10109[hep-ph]
[69] V. I. Telnov, Nucl. Instrum. Meth. A **294**, 72 (1990)
[70] A. Denner and S. Dittmaier, Nucl. Phys. B **734**, 62 (2006)
[71] T. Hahn and M. Perez-Victoria, Comput. Phys. Commun. **118**, 153 (1999), arXiv: 9807565[hep-ph]